ELSEVIER

Neurobiology of Aging 29 (2008) 1874–1893

NEUROBIOLOGY OF AGING

www.elsevier.com/locate/neuaging

# Aging elevates metabolic gene expression in brain cholinergic neurons☆

Karen A. Baskerville [a], Caroline Kent [a], David Personett [a], Weil R. Lai [b], Peter J. Park [b], Paul Coleman [c], Michael McKinney [a,*]

[a] *Department of Molecular Pharmacology and Therapeutics, Mayo Clinic Jacksonville, 4500 San Pablo Road, Jacksonville, FL 32224, United States*
[b] *Harvard-Partners Center for Genetics and Genomics, 77 Ave. Louis Pasteur, Boston, MA 02115, United States*
[c] *University of Rochester, School of Medicine and Dentistry, 601 Elmwood Ave., Box 645, Rochester, NY 14642, United States*

Received 1 March 2007; received in revised form 26 April 2007; accepted 27 April 2007
Available online 11 June 2007

**Abstract**

The basal forebrain (BF) cholinergic system is selectively vulnerable in human brain diseases, while the cholinergic groups in the upper pons of the brainstem (BS) resist neurodegeneration. Cholinergic neurons (200 per region per animal) were laser-microdissected from five young (8 months) and five aged (24 months) F344 rats from the BF and the BS pontine lateral dorsal tegmental/pedunculopontine nuclei (LDTN/PPN) and their expression profiles were obtained. The bioinformatics program SigPathway was used to identify gene groups and pathways that were selectively affected by aging. In the BF cholinergic system, aging most significantly altered genes involved with a variety of metabolic functions. In contrast, BS cholinergic neuronal age effects included gene groupings related to neuronal plasticity and a broad range of normal cellular functions. Transcription factor GA-binding protein alpha (GABPα), which controls expression of nuclear genes encoding mitochondrial proteins, was more strongly upregulated in the BF cholinergic neurons (+107%) than in the BS cholinergic population (+40%). The results suggest that aging elicits elevates metabolic activity in cholinergic populations and that this occurs to a much greater degree in the BF group than in the BS group.


*Keywords:* Aging; Gene expression; Acetylcholine; Basal forebrain; Neuronal vulnerability; Metabolic genes; Bioinformatics

## 1. Introduction

In several human brain diseases, including Alzheimer's disease (AD), the basal forebrain cholinergic system degenerates (McKinney and Coyle, 1991; McKinney, 2005). This complex of neurons innervates cortex, hippocampus and amygdala, where deposits of abnormal amyloid are found in AD and Down Syndrome. Genetic studies of AD have found specific mutations in the amyloid precursor protein and presenilin that co-segregate with the early onset form of the disease, which occurs in a minority of AD patients. These genetic data, when considered in conjunction with numerous findings of neurotoxic effects of amyloid protein fragments, seems to strongly support the hypothesis that dysfunction in amyloid metabolism is the cause of AD. But, the basal forebrain cholinergic complex also degenerates in a variety of other human brain diseases, in which excessive amyloid deposition does not occur. Moreover, cerebral amyloid plaques occur in normal human aging. In transgenic models of amyloid deposition, cholinergic degeneration does not occur (Hernandez et al., 2001; reviewed in McKinney, 2005). We, and others, have proposed that excessive oxidative stress may be the primary pathological condition in AD.

The pons of the brainstem contains several cholinergic groups lying within the core reticular region, notably the laterodorsal tegmental nucleus (LDTN) and the pedunculopontine nucleus (PPN), that have functional and anatomical

☆ This paper is dedicated to the memory of Dr. Amandip K. Utal, Ph.D., friend and colleague.

* Corresponding author. Tel.: +1 904 953 8713; fax: +1 904 953 7117.
*E-mail address:* mckinney@mayo.edu (M. McKinney).

0197-4580/$ – see front matter © 2007 Elsevier Inc. All rights reserved.
doi:10.1016/j.neurobiolaging.2007.04.024

relationships with the basal forebrain system (McKinney et al., 2003). These neurons seem to be preserved in AD (Woolf et al., 1989). In vitro studies comparing responses of cholinergic neurons after exposure to nitrosative or oxidative stress have demonstrated that the pontine cholinergic neurons are remarkably resistant to these stressors, while the basal forebrain cholinergic neurons are relatively more vulnerable (Fass et al., 2000; McKinney et al., 2004). These findings are consistent with a selective vulnerability of the basal forebrain complex in aging. Consistent with this hypothesis, we recently documented a selective partial loss of this population in aged Long-Evans rats (Baskerville et al., 2006). Selective vulnerability in "normal" aging can provide valuable clues as to how neuronal populations might respond to disease processes. Probably the major force applied to biological systems in aging is oxidative stress, and this is likely to be even more important for the brain, given its relatively great demand for oxygen and energy substrates. There may be further elevation of oxidative stress in age-related diseases like AD and PD.

A protocol for linear amplification of sub-femtogram levels of mRNA to microgram levels using the RNA polymerase of phage T7 was originally devised by Eberwine and colleagues (Van Gelder et al., 1990), making possible the microarray profiling of a few, or even single, cells (Cheetham et al., 1997; Chow et al., 1998). Microdissection methodologies have been well established over more than a decade of experimentation, but genome-wide profiling of microdissected populations began with a seminal paper addressing two neuronal morphological types in the dorsal root ganglion (Luo et al., 1999). Microdissection protocols have matured since that time and have become much more widespread in their application; they now include studies of neuronal types in brain tissue (Bonaventure et al., 2002; Chung et al., 2005). We adapted these novel technologies specifically to the question of determining age effects on brain cholinergic populations.

## 2. Methods

### 2.1. Experimental subjects

Young (8 months) and aged (24 months) F344 rats were ordered from the National Institute on Aging. There were five (5) animals in each group for this study. Animal handling procedures were authorized by an approved Institutional Animal Care and Use Committee protocol. Subjects were euthanised by decapitation and the brains were blocked coronally and frozen on to chucks for sectioning.

### 2.2. Laser-assisted microdissection of cholinergic populations

Sections (10 μm) were obtained with a Leica CM3050S cryostat and mounted on metal foil slides (Leica). Sections were fixed with ice-cold acetone, dehydrated with ethanol and dried. Immunocytochemical visualization of cholinergic neurons was performed under RNAse-free conditions (using 500 units/mL RNAsin, Promega) with a 1:1000 dilution of goat polyclonal primary antibody to choline acetyltransferase (Chemicon International, AB144P), followed by incubation with a biotinylated rabbit anti-goat secondary antibody. Extravidin (Vector Laboratories, 1:1000) was added and the antibody complex was visualized by reaction with hydrogen peroxide and diaminobenzidine (Sigma Chemical Company). Two hundred (200) cholinergic neurons were microdissected from the basal forebrain (BF) region (medial septum, diagonal band) and brainstem (BS) pontine region (laterodorsal tegmental nucleus, LDTN; pedunculopontine nucleus, PPN). The neurons were collected in the caps of sterile PCR tubes containing RNAse extraction buffer. Total RNA was extracted from the BF and BS microdissected populations using a kit (Picopure, Arcturus). RT-PCR was performed on a portion of the RNA preparation in order to verify quality; microdissections were repeated until a full set of 20 samples (10 basal forebrain; 10 brainstem) with quality RNA was obtained.

### 2.3. Microarray protocols

The mRNA was amplified in a two-stage T7 RNA polymerase-based method with a kit from Arcturus Engineering (RiboAmp HS RNA Amplification Kit). In the second stage, the synthesis of aRNA (amplified RNA) involved incorporation of amino-allyl UTP residues. The aRNA preparations were labeled either with Alexa Fluor 555 (samples from young subjects) or Alexa Fluor 647 (samples from aged subjects) from Molecular Probes (Eugene, OR). Self–self hybridization studies comparing the cyanine-based dyes with the Alexa series indicate relatively little dye bias for the latter chemistry (Cox et al., 2004). A two-color microarray protocol was designed in which young and aged samples were contrasted within each region (BF or BS). The hybridization protocol was performed so that comparisons between BF and BS would have identical dye bias, if any. Thus, regionally selective age effects will not be confounded by dye bias effects. The labeled samples were hybridized to Agilent Rat Oligo 60-mer microarrays in Agilent microarray chambers (G2534A) at 60° for 17 h.

### 2.4. Bioinformatics methods

The arrays were scanned in a confocal laser scanner (ScanArray Express, Packard Bioscience, Perkin-Elmer) and Imagene software (version 6; BioDiscovery, Inc.) was used to process the images. Data were imported into GeneSpring (version 7.2, Silicon Genetics, Perkin-Elmer) for exploratory analyses. Both "global" and LOWESS normalization were performed, the former to directly compare BF versus BS and the latter to compare age effects in BF and BS. In the global method, each channel (dye) was considered independent. In the LOWESS method, the ratios of the two channels on each array are adjusted to correct for possible dye bias as well

as non-linearity between transcript levels and signal intensity. A total of 10 arrays (20 channels) were processed (five young BF versus five aged BF; five young BS versus five aged BS). That is, on each array the two channels contrasted a young sample with an aged sample from the same brain region. The data were exported into Microsoft Excel, then to Star Calc, and saved in "comma-separated value" format. For pathway analysis, the data were imported into *R* (version 2.2.1; http://www.r-project.org) and analyzed with the SigPathway package (Tian et al., 2005; version 1.1.3, available as a Bioconductor package at http://www.bioconductor.org). Evaluations of the data included comparing results for gene sets in which genes were present in all 20 channels with gene sets with missing values imputed by the K-nearest neighbor method (Troyanskaya et al., 2001). For LOWESS processed data, up to four missing values were imputed; for globally normalized data up to two missing values were imputed. The SigPathway package performs "pathway analysis" on microarray data by grouping genes on the microarray according to their ontological classifications, and using permutation methods to determine two statistical parameters, $NE_k$ and $NT_k$, for the *k*th gene set. $NE_k$ is a measure of the degree to which a given geneset has a composite expression differing from other genesets on the array; $NT_k$ is a measure of the degree to which the geneset composite expression is different between phenotypes (across arrays). The program ranks gene ontology groups according to the average of the rank-orders of *q*-values for $NE_k$ and $NT_k$. Because each of the two measures can give false positive gene sets, we require that the rank be high in both. For the primary discussion of regionally selective age effects, we used the LOWESS-normalized microarray data. To demonstrate "basal" gene expression differences between the BF and BS (i.e., in the young groups), we used the "single-channel" processed (globally normalized) dataset. The validity of analyzing channels independently has been discussed previously (Park et al., 2004; Attoor et al., 2004). It appears that even though the hybridization is competitive, the amount of spotted probes is sufficiently large that the hybridization in each channel is nearly independent. Independence of the two channels when using current microarray technology is observable over a wide range of probe concentrations (Wang et al., 2002). Moreover, in our analysis, we concentrate at the level of pathways rather than independent genes. Because this analysis is more robust, noise in the expression levels of individual genes due to the violation of the independence assumption will have relatively little impact on the outcome of the analysis.

### 2.5. Dual immunocytochemistry for choline acetyltransferase and GA-binding protein α

Sections (20 μm) were cut from the same brain blocks used for the microarray experiments and fixed with acetone for 6 min. Choline acetyltransferase (ChAT) staining was performed first, using a 1:400 dilution of a goat anti-CAT primary antibody (AB144P, Chemicon) and a 1:400 dilution of a biotinylated rabbit anti-goat secondary antibody (Vector). The ChAT immunoreactivity was visualized with ExtrAvadin (1:1000, Sigma E-2886), hydrogen peroxide and diaminobenzine (brown product). Before conducting GABPa staining, residual peroxidase activity was blocked using two washes in 3% hydrogen peroxide in 10% methanol (30 min). A 1:100 dilution of a rabbit polyclonal primary antibody for GABPα (sc-22810, Santa Cruz Biotechnology) and a 1:200 dilution of a biotinylated goat anti-rabbit secondary antibody (BA-1000, Vector), with visualization by ExtrAvidin, hydrogen peroxide and diaminobenzidine with nickel-enhancement (blue-black product). Sections were mounted, dehydrated, cleared with xylene and coversliped with Cytoseal 60 (Richard-Allan Scientific).

### 2.6. Quantitative real-time PCR (qRT-PCR) protocol

The RNA extracted from 200 neurons was used entirely for the amplification, except for a fraction used to perform a quality check for RNA integrity (RT/PCR for GAPDH mRNA). Validation of microarray results was performed for nine genes on aRNA transcribed from double-stranded (ds) cDNA from the second stage of T7 amplification (one-half of the ds cDNA was reserved for microarray work; the other half for PCR). The aRNA produced in this reaction was converted to cDNA using reverse transcriptase and random hexamer priming. First-strand cDNA synthesis of 2 μg of amplified transcripts (aRNA, see in vitro transcription method above) was carried out according to kit instructions (Invitrogen, Calsbad, CA, random primer method) with slight modifications to the protocol. We found that cDNA synthesis of aRNA improved when the incubation temperature was increased from 50 to 55 °C. Twelve (12) microliters of a qRT-PCR reagent master mix (SuperArray, Fredrick, MD) [6.25 μL SYBR Green PCR Master Mix, 0.5 μL appropriate primer set and 5.25 μL molecular biology-grade water (Eppendorf, Westbury, NY) per reaction] were combined in a nucleic acid-, nuclease-free microfuge tube (Ambion, Austin, TX), mixed in an sterile round-bottomed polystyrene microtiter plate well (Greiner Bio-One, Durham, NC) containing 1 μL cDNA and subsequently transferred to a 384-well Clear Optical Reaction Plate (ABI Prism, Foster City, CA). The reaction was performed according to the company protocol (SuperArray) for all primer sets with a slight modification: 95 °C, 15 min; then 95 °C, 30 s; 55 °C, 30 s; 72 °C, 45 s for 50 cycles. Real-time PCR amplicon detection was performed on an ABI Prism Sequence Detection System, model 7900HT, and the data captured with the ABI Prism SDS v2.1 software. Nine primer sets (SuperArray) targeting the following mitochondrial-related gene transcripts of interest: Arf-3 (NM_080904), Atp5e (NM_139099), Atp5j (NM_053602.1), Atp5o (NM_138883), Atp6l (NM_130823), Cox5a (NM_154783), Cox6c (NM_019360), HSPe1 (NM_012966), Tfam (NM_031326) and GAPDH (NM_117008). Log serial dilutions of pooled cDNA samples were assayed by PCR to determine amplification efficiencies

for the genes of interest and the "housekeeping" gene GAPDH. Threshold cycle ($C_t$) values were extrapolated by the Prism software to quantify relative gene expression values using the $2^{-DDC_t}$ method (Livak and Schmittgen, 2001**). For amplification efficiencies found to be less than 100%, $C_t$ values were calculated by using the following equation:

$$10^{[(-DDC_t/(\text{slope(gene)} + \text{slope(GAPDH)}/2)]}$$

## 3. Results

### 3.1. Exploratory cluster analysis

In our experiments, each microarray was co-hybridized with an aged sample (labeled with Alexa 647, or "red" dye) and with a young sample (labeled with Alexa 555, or "green" dye) from same region (BF or BS). The Alexa dyes are reported to have minimal "dye bias" (Cox et al., 2004), but this experimental layout would equate any such bias between the BS and BF regions, so that comparisons of age effects between the two regions would not be confounded.

We processed our experimental data so we could use two different methods of analyzing it. In conventional two-color microarray approaches, effects of variations in spot geometry and dye incorporation are removed by analyzing the *ratios* of channel intensities (i.e., a signal of interest in one channel, e.g., the aged sample, is compared with a reference or control signal in the other channel, e.g., the young sample). Use of the ratio approach in the current experimental design limits the analysis to comparison of *age effects* between the two brain regions. Non-linearity in the intensity plot (Channel 2 versus Channel 1, plotted logarithmically) is removed with an empirical method called the *LOWESS* (*LO*cally *WE*ighted polynomial regre*SS*ion) transformation.

In the other method of data analysis, which we call the "*single channel*" method, the two channels of each array are treated independently. The 20 individual channels of the 10 arrays are normalized to equivalent overall intensities (using the intensities of all the genes in the channel), and then these normalized intensities of each gene are expressed as fractions of the average intensity across all 20 channels. This is called "*global*" normalization because all the genes, rather than "housekeeping" genes, in each channel are used in adjusting the intensities between channels or samples. After normalization, an expression value greater than 1.0 indicates a relatively higher expression for that gene in that sample, as compared with all the samples in the experiment. The effect of aging can be calculated by dividing the normalized values for the aged samples by the normalized values for the young samples, in a given region (BF or BS).

Unsupervised clustering of LOWESS-normalized ratio data or globally normalized single channel data (12,166 genes; present in at least 18 of 20 channels) was performed with GeneSpring 7.2 using the Pearson correlation (Fig. 1A and B). In the tree for LOWESS-normalized data (Fig. 1A), the upper major cluster (labeled "I") represents genes most

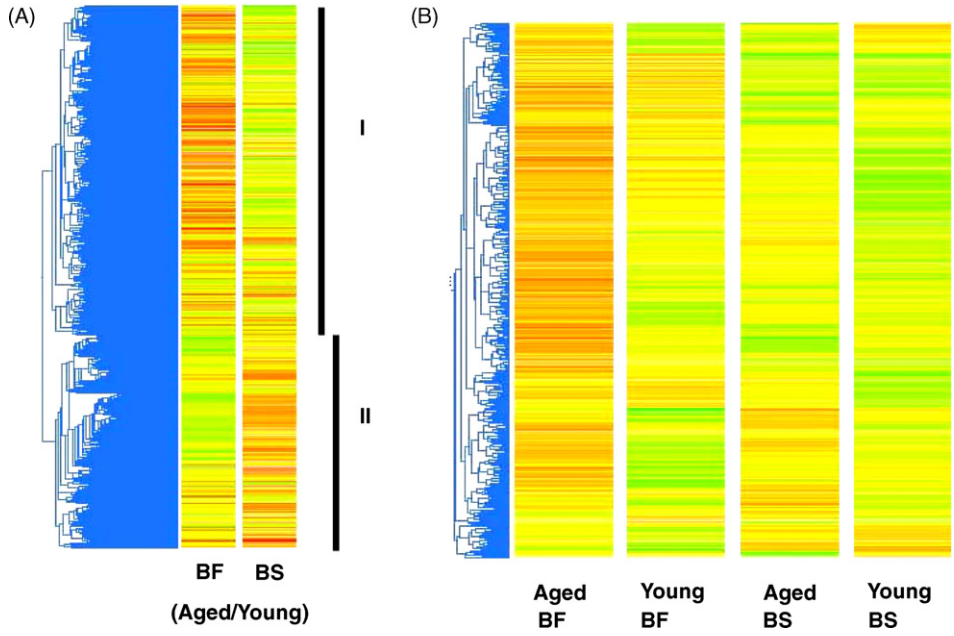


Fig. 1. Cluster analysis of cholinergic microarray data. Two-color microarray hybridization experiments were performed with Alexa dye-labeled T7-amplified aRNA from 200 neurons microdissected from the BF or BS of five young (8 months) and five aged (24 months) F344 rats. The cluster analysis shown at A was performed on LOWESS-normalized data (ratios of aged/young, paired on 10 arrays). The two major clusters in A discussed in the text are marked with vertical bars along the right side (I, most genes upregulated in aged BF; II, most genes upregulated in aged BS). The cluster analysis at B was performed on globally normalized "single channel" data (each subject/channel treated independently). The genes shown are those present in all 20 channels (∼4800). The GeneSpring program (v. 7.2) was employed; the metric was the Pearson correlation. Warmer colors in the left-hand analysis represent upregulation by aging; warmer colors in the right-hand analysis represent higher normalized gene levels.

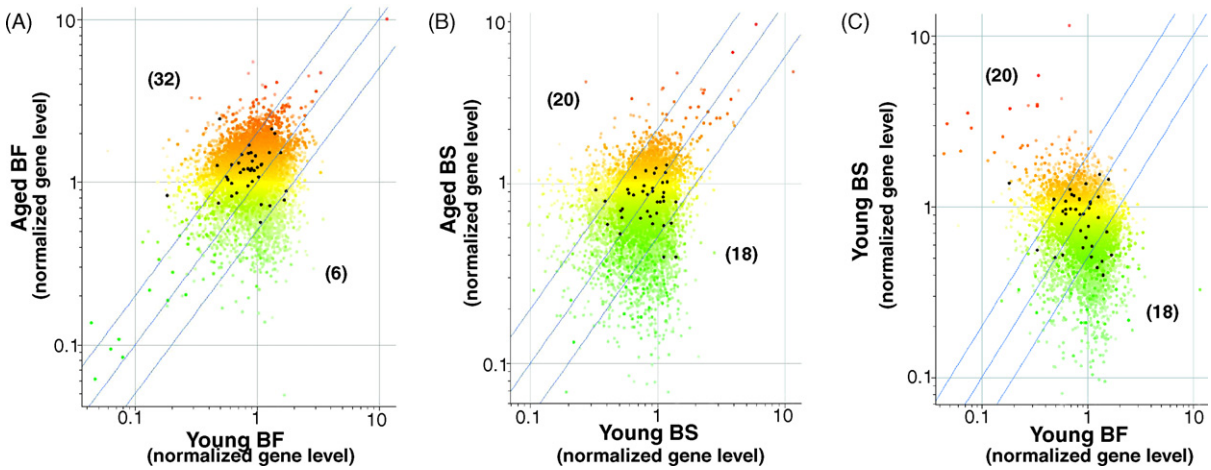


Fig. 2. Evidence for regionally selective age-induced upregulation of a metabolic gene set in young and aged BF and BS cholinergic neurons. The colored dots plot normalized expression levels ("1" indicates the mean level across all 20 channels) of genes that were present in at least 10 of 20 channels of the 10 microarrays. The warmer colors indicate higher levels (RED = up to five-fold or more over mean), while the cooler colors indicate expression levels below the mean (GREEN = down to one-fifth of the mean). Each plot in A, B or C is colorized according to the range of values for the phenotype plotted on the vertical axis. The central blue diagonal line represents equivalent expression for the two phenotypes plotted on the X and Y axes, while the two other blue diagonal lines indicate expression levels that are two-fold higher or lower. A text search for genes annotated with "mitochond*" with "oxido*" and "reduc*" collected 38 genes (levels shown as black dots), and these are overlaid on the total gene set (in color). The black numbers in parentheses indicate those genes in the "mitochondrial oxidoreductases" set that are above or below the line of equivalent expression.

of which were upregulated by aging in the BF, relative to BS genes. The lower major cluster (labeled "II") represents genes that were mainly increased by aging to a greater degree in the BS than in the BF. In the globally normalized data (Fig. 1B), with which individual channels were analyzed, it is evident that the effect of age is much more pronounced in the BF than in the BS.

In exploratory analysis of the globally normalized data, two-way analysis of variance (ANOVA; $p < 0.05$, no correction for multiple testing) indicated 739 genes were altered by *Age*, 1456 genes differed by *Tissue Type* (BF versus BS) and 238 genes were significant in the *Age* × *Tissue Type* interaction. Perusal of the 739 genes affected by *Age* indicated many ribosomal and metabolism-related genes (e.g., cytochrome oxidase or ATPase subunits). In a *t*-test for age effects in the BF, 572 genes were significant ($p < 0.05$; no correction for multiple testing). Many of these genes were located in clusters in which age effects were much more pronounced (mainly upregulation) for the BF than for the BS. Again, it was noted that many of these genes were related to ribosome structure or metabolism. In a *t*-test for age effects in the BS, 188 genes were significant at $p < 0.05$. Only 21 of these were also in the list of 572 genes significantly changed by age in the BF. Of these, only one gene (NM_053502, ATP-binding cassette Abcg1) was a metabolic gene; this is an ATPase that may be involved in cholesterol transport (Hoekstra et al., 2003).

### 3.2. Exploratory scatterplot analysis

Further exploration addressing metabolic and ribosomal genes was performed using scatterplots of the globally normalized data in GeneSpring. Searches of annotations for genes fitting selected ontological categories were performed with this program. Fig. 2 shows comparisons of age effects in BF and BS, and a comparison of young BF with young BS, with a set of "mitochondrial oxidoreductases" genes (38 genes, shown in black) superimposed on all of the normalized data (12,166 genes, shown in color). An age effect predominating in the BF is evident in these data: Fig. 2A shows that the majority of this group of genes plots above the diagonal line of equivalent expression in the BF, while in the BS (Fig. 2B) they are nearly equally distributed above and below the line (the black numbers shown in parentheses in these figures indicate the number of mitochondrial oxidoreductase genes above or below the diagonal line of equivalent expression). In the comparison of young BF and young BS (Fig. 2C), these genes are also roughly equally distributed above and below the line of equivalency, as would be expected in the comparison of constitutive genes between two normal tissue types. These patterns of expression were also seen with several other gene sets related generically to "mitochondrial", "electron transport" and "mitochondrial ribosomal" ontologies (not shown). In all cases, the comparisons of young BF with young BS showed equal, or nearly equal, distributions of genes in the sets above and below the lines of equivalency, and a relative upregulation of expression level in BF but not BS.

This exploration of the data indicates that dye bias cannot explain the age effects in the BF. Moreover, gene ontologies that were not mitochondrial or energy related did not exhibit the BF age effect (distributions were symmetrical for these plots; not shown). Thus, these preliminary analyses suggest that aging induces some kind of upregulation of genes associated with mitochondrial function and/or energy production in the cholinergic group of the BF, to a greater degree than in the BS group.

An examination of the LOWESS-normalized data gave similar findings. For example, using the list of genes (4841) which were deemed expressed in all channels of the 10 arrays, a search for annotations related to "mitochondria" yielded 111 genes, of which 60 were more strongly upregulated by aging in the BF and 23 were more strongly upregulated in BS. These aging-induced genes included subunits of cytochrome oxidase, ATPase and mitochondrial ribosomes. For example, the 25 mitochondrial ribosomal proteins in this dataset averaged a normalized level of $1.15 \pm 0.08$ for the BF and $0.88 \pm 0.05$ for the BS ($p < 0.01$). Also of note were increases caused by aging in BF of manganese superoxide dismustase (NM_017051; BF = 1.226, BS = 0.702), the mitochondrial import system, mitochondrial transcription factor A (NM_031326; BF = 1.504, BS = 0.376; Fig. 3) and the mitochondrial transcription termination factor 1 (NM_053499; BF = 1.382, BS = 1.041; Fig. 4). While these age effects are modest, typically in the range of 15–50% above young levels, the consistency of upregulation in BF, as opposed to BS, indicates a systematic effect on the rostral cholinergic system.

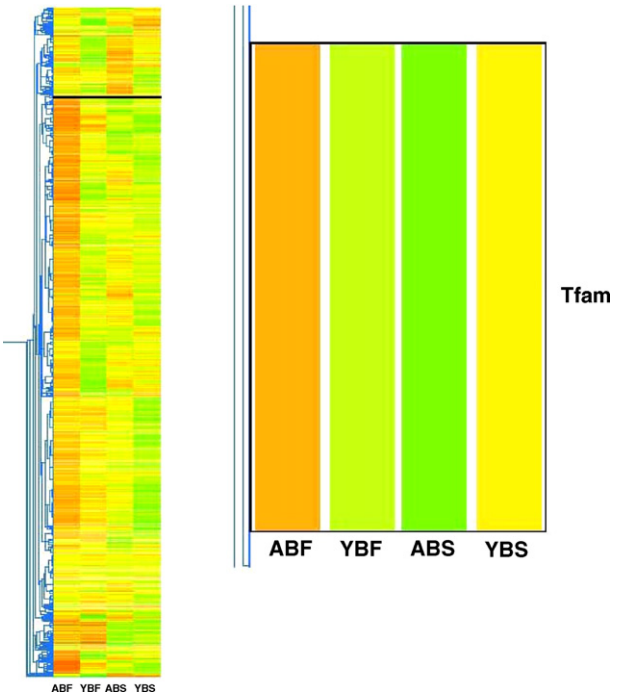


Fig. 3. Expression of mitochondrial transcription factor A (NM_031326) in young and aged BF and BS cholinergic neurons. GeneSpring (v. 7.2) was used to cluster the globally normalized genes present in all 20 channels of the 10 microarrays. There were five aged and five young F344 rats in the experiment, and their normalized genes were averaged and displayed. The cluster location of mitochondrial transcription factor A (Tfam) is shown at left, and the levels of Tfam mRNA in each biological group are shown at right. Warmer colors represent levels above 1.0; cooler colors are for levels below 1.0. The color scale runs from green (five-fold lower) to red (five-fold higher). These data indicate that aging caused this gene to be upregulated in BF and downregulated in BS.

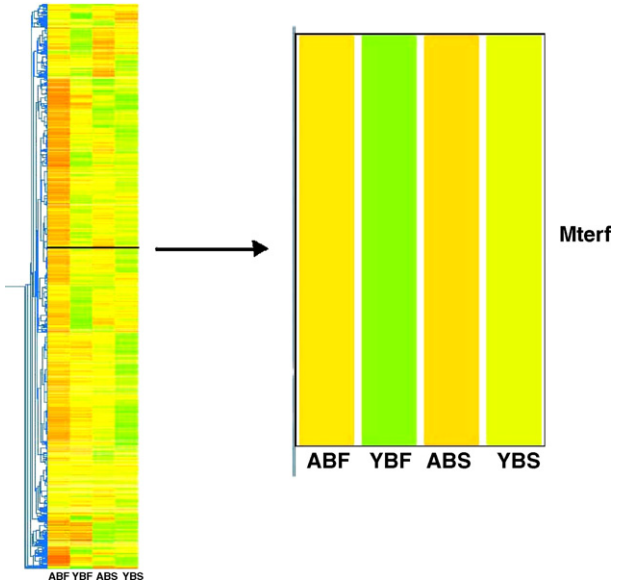


Fig. 4. Expression of mitochondrial transcription termination factor 1 (NM_053499) in young and aged BF and BS cholinergic neurons. GeneSpring (v. 7.2) was used to cluster the globally normalized genes present in all 20 channels of the 10 microarrays (five young and five aged F344 rats). The location of mitochondrial transcription termination factor A (Mterf) is shown at left, and the levels in each biological group are shown at right. Warmer colors represent levels above 1.0; cooler colors are for levels below 1.0. The color scale runs from green (five-fold lower) to red (five-fold higher). This mRNA was increased by aging in both BF and BS populations.

### 3.3. Pathway discovery

Analysis of microarray data using classical statistical methods often produces results that are "unfocused from a biological point of view" (Lottaz and Spang, 2005). However, it is being increasingly realized that biological insight is readily achievable by use of a priori established gene sets to perform "structured analysis" of microarray data (Bild and Febbo, 2005; Curtis et al., 2005). One of the more successful methods of this type of analysis is that of "*G*ene *S*et *E*nrichment *A*nalysis" (GSEA; Mootha et al., 2003). Recently, one of our laboratories developed an improvement on the GSEA method for discerning expression effects on gene ontological of signaling groupings in microarray data, called "SigPathway" (Tian et al., 2005). This approach is statistically more rigorous because it eliminates biases due to size or the correlation structure of the gene set; additionally, it incorporates several pathway databases with gene ontology databases. This program, written for execution in the "*R*" statistical package (http://cran.r-project.org/), was used to determine the effects of aging on the microarray data for BF and BS cholinergic populations. We analyzed young and aged BS and BF microarray data normalized both by the LOWESS method (on ratios of "Aged/Young", the two channels in each array), and the same data normalized globally as "single channels" (each channel/sample treated independently). The former method might be considered the "traditional"

Table 1
Pathway analysis of LOWESS-normalized microarray data for microdissected BF and BS cholinergic populations

| Combined rank | Gene set category | Pathway | Set size | Percent up | $NT_k$ stat | $NT_k$ rank | $NE_k^*$ stat | $NE_k^*$ rank |
|---|---|---|---|---|---|---|---|---|
| 1 | GO:0005839 | Proteasome core complex (sensu Eukaryota) | 15 | 87 | 4.08 | 7 | 4.43 | 1 |
| 2 | KEGG:rno03050 | Proteasome | 21 | 81 | 3.72 | 14 | 4.1 | 2 |
| 3 | GO:0000502 | Proteasome complex (sensu Eukaryota) | 23 | 78 | 3.61 | 20 | 4.02 | 3 |
| 4 | GO:0005829 | Cytosol | 163 | 67 | 5.16 | 1 | 3.1 | 28 |
| 5 | GO:0005783 | Endoplasmic reticulum | 163 | 66 | 4.38 | 3 | 3.08 | 32 |
| 6 | GO:0005489 | Electron transporter activity | 78 | 69 | 3.85 | 11 | 3.16 | 25 |
| 7 | GO:0005871 | Kinesin complex | 42 | 67 | 3.5 | 27 | 3.31 | 11 |
| 8 | GO:0007010 | Cytoskeleton organization and biogenesis | 138 | 59 | 3.3 | 33 | 3.22 | 20 |
| 9 | GO:0005773 | Vacuole | 38 | 74 | 3.09 | 49.5 | 3.46 | 8 |
| 10 | GO:0007420 | Brain development | 25 | 28 | −3.6 | 21 | −3.02 | 40 |
| 11 | GO:0005875 | Microtubule associated complex | 71 | 62 | 3.09 | 49.5 | 3.23 | 18 |
| 12 | GO:0005764 | Lysosome | 33 | 70 | 2.88 | 66 | 3.58 | 6 |
| 13 | GO:0000323 | Lytic vacuole | 33 | 70 | 2.88 | 66 | 3.58 | 6 |
| 14 | GO:0006091 | Generation of precursor metabolites and energy | 177 | 58 | 3.56 | 23 | 2.93 | 63 |
| 15 | GO:0016684 | Oxidoreductase activity, acting on peroxide as acceptor | 11 | 73 | 2.65 | 84 | 3.78 | 4 |
| 16 | GO:0004601 | Peroxidase activity | 11 | 73 | 2.65 | 84 | 3.78 | 4 |
| 17 | GO:0016209 | Antioxidant activity | 18 | 78 | 2.65 | 84 | 3.38 | 10 |
| 18 | GO:0009141 | Nucleoside triphosphate metabolism | 29 | 86 | 3.63 | 18 | 2.7 | 112 |
| 19 | KEGG:rno00190 | Oxidative phosphorylation | 44 | 75 | 3.98 | 8 | 2.65 | 144 |
| 20 | GO:0007229 | Integrin-mediated signaling pathway | 15 | 33 | −2.07 | 138 | −3.24 | 16 |
| 21 | GO:0009199 | Ribonucleoside triphosphate metabolism | 24 | 88 | 3.72 | 15 | 2.65 | 144 |
| 22 | GO:0009205 | Purine ribonucleoside triphosphate metabolism | 24 | 88 | 3.72 | 15 | 2.65 | 144 |
| 23 | GO:0006511 | Ubiquitin-dependent protein catabolism | 44 | 59 | 1.98 | 155 | 3.72 | 5 |
| 24 | GO:0019941 | Modification-dependent protein catabolism | 44 | 59 | 1.98 | 155 | 3.72 | 5 |
| 25 | GO:0015036 | Disulfide oxidoreductase activity | 11 | 73 | 1.98 | 155 | 3.43 | 9 |
| 26 | GO:0007411 | Axon guidance | 24 | 54 | 2 | 150.5 | 3.27 | 14 |
| 27 | GO:0006164 | Purine nucleotide biosynthesis | 31 | 81 | 3.56 | 22 | 2.65 | 144 |
| 28 | GO:0001525 | Angiogenesis | 18 | 61 | 1.9 | 168.5 | 3.29 | 12 |
| 29 | KEGG:rno00193 | ATP synthesis | 17 | 88 | 3.67 | 16 | 2.6 | 204 |
| 30 | GO:0009144 | Purine nucleoside triphosphate metabolism | 25 | 88 | 3.82 | 12 | 2.52 | 219 |
| 31 | GO:0006119 | Oxidative phosphorylation | 30 | 80 | 3.95 | 9 | 2.49 | 224 |
| 32 | GO:0003735 | Structural constituent of ribosome | 75 | 79 | 4.83 | 2 | 2.41 | 249 |
| 33 | GO:0006163 | Purine nucleotide metabolism | 33 | 82 | 3.88 | 10 | 2.41 | 249 |
| 34 | GO:0009986 | Cell surface | 20 | 65 | 1.53 | 244 | 3.23 | 19 |
| 35 | GO:0008081 | Phosphoric diester hydrolase activity | 17 | 41 | −1.52 | 247 | −3.24 | 17 |
| 36 | GO:0009150 | Purine ribonucleotide metabolism | 29 | 83 | 3.62 | 19 | 2.41 | 249 |
| 37 | GO:0046034 | ATP metabolism | 19 | 84 | 3.54 | 24 | 2.41 | 249 |
| 38 | GO:0015399 | Primary active transporter activity | 65 | 71 | 3.66 | 17 | 2.26 | 303 |
| 39 | GO:0048514 | Blood vessel morphogenesis | 21 | 52 | 1.15 | 333 | 3.52 | 7 |
| 40 | GO:0046943 | Carboxylic acid transporter activity | 23 | 52 | −0.98 | 386.5 | −3.28 | 13 |
| 41 | GO:0005342 | Organic acid transporter activity | 23 | 52 | −0.98 | 386.5 | −3.28 | 13 |
| 42 | GO:0005840 | Ribosome | 75 | 76 | 4.26 | 4 | 1.59 | 446.5 |
| 43 | GO:0030529 | Ribonucleoprotein complex | 129 | 69 | 4.11 | 6 | 1.59 | 446.5 |
| 44 | KEGG:rno03010 | Ribosome | 41 | 90 | 4.17 | 5 | 1.46 | 481.5 |
| 45 | GO:0005830 | Cytosolic ribosome (sensu Eukaryota) | 38 | 87 | 3.81 | 13 | 1.46 | 481.5 |
| 46 | GO:0001568 | Blood vessel development | 22 | 50 | 0.7 | 487 | 3.25 | 15 |
| 47 | GO:0001944 | Vasculature development | 22 | 50 | 0.7 | 487 | 3.25 | 15 |

GeneSpring (v. 7.2) was used to normalize the microarray data by the LOWESS method and the files were exported to Excel where those genes expressed in at least 9 out of 10 arrays were formatted for import into *R* (v. 2.2.1). The data represent the ratio of Channel 2/Channel 1, which in all cases is aged/young. Missing values were imputed and the SigPathway program was used to rank gene sets according the average of the $NT_k$ and $NE_k$ statistics. "Set Size" indicates the number of genes in the "GO" or "KEGG" ontologies. In this analysis "Percent Up" indicates the percentage of genes in the set that were more greatly increased by age in the BF phenotype.

approach to two-color array analysis, while the utility of the latter method has been less recognized.

There were many more effects of aging in the BF, as compared with the BS, as Fig. 1 vividly shows. Moreover, the majority of effects involved upregulation of expression. There were also major qualitative differences between BF and BS gene level changes, that were evident in the SigPathway analyses and as suggested by the exploratory analyses shown in Figs. 2–4. The SigPathway results are given in Table 1 (for LOWESS normalized data) and in Table 2 (BF) and Table 3 (BS) for globally normalized "single channel" data.

In the data processed by the LOWESS method, aged/*young* ratios report the effect of aging on a given phenotype (BF or BS): a value above unity (1) indicates an age effect. The data in Table 1 identify numerous gene ontology groups for which the effects of aging are significantly different between the two phenotypes. In most of the gene sets in

Table 2
Pathway analysis for the BF cholinergic population using single channel data

| Combined rank | Gene set category | Pathway | Set size | Percent up | $NT_k$ stat | $NT_k$ rank | $NE^*_k$ stat | $NE^*_k$ rank |
|---|---|---|---|---|---|---|---|---|
| 1 | GO:0016469, 6753, 6754, 15985, 15986, 46961, 46933 | ATP metabolism | 18 | 6 | −3.09 | 6.5 | −3.15 | 1 |
| 2 | GO:0046034 | ATP metabolism (plus 1 gene) | 19 | 5 | −3.09 | 6.5 | −3.12 | 2 |
| 3 | GO:0006752 | ATP metabolism (plus 1 gene) | 19 | 5 | −2.88 | 13.5 | −3.09 | 4 |
| 4 | GO:0030140 | Trans-Golgi network transport vesicle | 12 | 17 | −2.88 | 13.5 | −2.94 | 16 |
| 5 | GO:0006725 | Aromatic compound metabolism | 24 | 4 | −2.65 | 21.5 | −2.99 | 10 |
| 6 | GO:0008565 | Protein transporter activity | 49 | 4 | −4.26 | 1 | −2.85 | 32 |
| 7 | GO:0016311 | Dephosphorylation | 36 | 3 | −2.88 | 13.5 | −2.9 | 24 |
| 8 | GO:0006818 | ATP metabolism (plus 5 genes) | 26 | 8 | −2.58 | 26 | −2.96 | 12 |
| 9 | GO:0009205 | Purine ribonucleoside triphosphate metabolism | 24 | 8 | −2.65 | 21.5 | −2.93 | 17 |
| 10 | GO:0015992 | Proton transport | 24 | 8 | −2.58 | 26 | −2.94 | 14 |
| 11 | GO:0016791 | Phosphoric monoester hydrolase activity | 61 | 10 | −3.24 | 4 | −2.81 | 38 |
| 12 | GO:0004721 | Phosphoprotein phosphatase activity | 41 | 5 | −2.88 | 13.5 | −2.85 | 31 |
| 13 | GO:0009141 | Nucleoside triphosphate metabolism (18 genes overlap with #23 or #29) | 29 | 7 | −2.41 | 41 | −3 | 9 |
| 14 | GO:0019829 | Cation-transporting ATPase activity | 26 | 15 | −2.41 | 41 | −2.94 | 15 |
| 15 | GO:0005764 | Lysosome | 33 | 12 | −2.88 | 13.5 | −2.75 | 52 |
| 16 | GO:0000323 | Lytic vacuole | 33 | 12 | −2.88 | 13.5 | −2.75 | 52 |
| 17 | GO:0009142 | Nucleoside triphosphate biosynthesis | 26 | 8 | −2.26 | 60.5 | −3.05 | 5 |
| 18 | GO:0005773 | Vacuole | 38 | 11 | −3.09 | 6.5 | −2.72 | 62 |
| 19 | GO:0042625 | ATPase activity, coupled to transmembrane movement of ions | 35 | 20 | −2 | 95 | −3.04 | 7 |
| 20 | GO:0015078 | Hydrogen ion transporter activity | 50 | 2 | −3.96 | 2 | −2.65 | 140 |
| 21 | GO:0045184 | Establishment of protein localization | 174 | 10 | −2.88 | 13.5 | −2.65 | 140 |
| 22 | GO:0015077 | Monovalent inorganic cation transporter activity | 54 | 6 | −2.88 | 13.5 | −2.65 | 140 |
| 23 | GO:0006119 | Oxidative phosphorylation (27 genes overlap with #29) | 30 | 3 | −3.09 | 6.5 | −2.62 | 201 |
| 24 | GO:0051325 | Interphase | 26 | 8 | −1.3 | 243.5 | −2.95 | 13 |
| 25 | GO:0006886 | Intracellular protein transport | 137 | 10 | −2.88 | 13.5 | −2.49 | 247 |
| 26 | GO:0016197 | Endosome transport | 11 | 18 | −1.23 | 265 | −3.1 | 3 |
| 27 | GO:0006650 | Glycerophospholipid metabolism | 11 | 0 | −1.24 | 260.5 | −3.02 | 8 |
| 28 | GO:0000086 | G2/M transition of mitotic cell cycle | 16 | 13 | −0.81 | 417.5 | −2.97 | 11 |
| 29 | KEGG:rno00190 | Oxidative phosphorylation (27 genes overlap with #23) | 44 | 5 | −3.35 | 3 | −2.26 | 427 |
| 30 | KEGG:rno04330 | Notch signaling pathway | 20 | 35 | 0.74 | 443 | −3.05 | 6 |
| 31 | GO:0004295 | Trypsin activity | 15 | 47 | 3.09 | 9 | −0.89 | 787 |
| 32 | GO:0004263 | Chymotrypsin activity | 12 | 42 | 2.75 | 18.5 | −1 | 783 |

Microdissected cholinergic neurons (200) from the BF of five young and five aged F344 rats were used for microarray analysis on Agilent Rat Oligo arrays (22,000 sequences). GeneSpring (v. 7.2) was used to "globally" normalize sets of genes expressed in at least 18 of 20 channels, treating each channel as an independent sample. The normalized data were exported to *R* and missing values were imputed before running SigPathway. The gene sets were ranked according to the average of $NT_k$ and $NE_k$ statistics. There was duplication of several of the ontologies, so these gene sets were collapsed. For example, the 18 genes in the top-ranked set were represented with identical statistics in seven GO groups; these seven are listed in "Gene Set Category" and the pathway was labeled "ATP metabolism". At other points in the table there was overlap in the genes contained in one or more GO groups, and this is indicated within parentheses.

Table 3
Pathway analysis for the BS cholinergic population using single channel data

| Combined rank | Gene set category | Pathway | Set size | Percent up | $NT_k$ stat | $NT_k$ rank | $NE_k^*$ stat | $NE_k^*$ rank |
|---|---|---|---|---|---|---|---|---|
| 1 | GO:0007214 | Gamma-aminobutyric acid signaling pathway | 10 | 0 | −2.88 | 6 | −2.65 | 1.5 |
| 2 | GO:0015036 | Disulfide oxidoreductase activity | 11 | 64 | 3.09 | 4 | 1.8 | 16 |
| 3 | GO:0045202 | Synapse | 42 | 17 | −2.75 | 9.5 | −1.91 | 13.5 |
| 4 | GO:0007031 | Peroxisome organization and biogenesis | 10 | 50 | 2.46 | 25 | 2.41 | 3 |
| 5 | GO:0016055 | Wnt receptor signaling pathway | 20 | 15 | −2.46 | 23 | −1.98 | 11 |
| 6 | GO:0045211 | Postsynaptic membrane | 14 | 7 | −2.29 | 35 | −2.26 | 6.5 |
| 7 | GO:0005179 | Hormone activity | 23 | 26 | −2.29 | 35 | −1.91 | 13.5 |
| 8 | GO:0042165 | Neurotransmitter binding | 19 | 16 | −2.17 | 43.5 | −1.91 | 13.5 |
| 9 | GO:0016917 | GABA receptor activity | 12 | 8 | −2.1 | 53.5 | −2.41 | 4.5 |
| 10 | KEGG:rno04510 | Focal adhesion | 47 | 21 | −2.03 | 60.5 | −1.8 | 17.5 |
| 11 | GO:0019200 | Carbohydrate kinase activity | 16 | 13 | −2.07 | 57 | −1.75 | 22 |
| 12 | GO:0004680 | Casein kinase activity | 17 | 12 | −2.01 | 63 | −1.8 | 17.5 |
| 13 | GO:0006766 | Vitamin metabolism | 10 | 0 | −1.91 | 76 | −1.75 | 22 |
| 14 | GO:0005184 | Neuropeptide hormone activity | 10 | 10 | −1.77 | 97 | −2.15 | 8.5 |
| 15 | GO:0003682 | Chromatin binding | 16 | 6 | −1.72 | 104 | −1.75 | 22 |
| 16 | GO:0004682 | Protein kinase CK2 activity | 13 | 15 | −1.71 | 106 | −1.75 | 22 |
| 17 | GO:0005249 | Voltage-gated potassium channel activity | 20 | 15 | −1.56 | 138.5 | −1.75 | 22 |
| 18 | GO:0004540 | Ribonuclease activity | 12 | 42 | 2.58 | 17 | 1.2 | 165.5 |
| 19 | GO:0008094 | DNA-dependent ATPase activity | 10 | 10 | −1.11 | 252.5 | −2.15 | 8.5 |
| 20 | GO:0008076 | Voltage-gated potassium channel complex | 15 | 20 | −1.15 | 240 | −1.75 | 22 |
| 21 | GO:0006695 | Cholesterol biosynthesis | 14 | 71 | 3.52 | 2 | 0.95 | 314.5 |
| 22 | GO:0006821 | Chloride transport | 15 | 27 | −0.88 | 346.5 | −2.41 | 4.5 |
| 23 | GO:0019201 | Nucleotide kinase activity | 10 | 30 | −0.76 | 397.5 | −2.65 | 1.5 |
| 24 | GO:0001525 | Angiogenesis | 18 | 44 | 2.58 | 17 | 0.75 | 458.5 |
| 25 | GO:0006487 | Protein amino acid N-linked glycosylation | 10 | 70 | 2.65 | 13 | 0.72 | 478 |
| 26 | GO:0005230 | Extracellular ligand-gated ion channel activity | 16 | 25 | −0.54 | 492 | −2.06 | 10 |
| 27 | GO:0016126 | Sterol biosynthesis | 17 | 71 | 3.5 | 3 | 0.65 | 532.5 |
| 28 | KEGG:rno00120 | Bile acid biosynthesis | 11 | 55 | 2.51 | 20.5 | 0.66 | 523.5 |
| 29 | GO:0019842 | Vitamin binding | 10 | 10 | −0.44 | 545.5 | −2.26 | 6.5 |
| 30 | GO:0007010 | Cytoskeleton organization and biogenesis | 138 | 34 | 2.51 | 20.5 | −0.6 | 567 |
| 31 | GO:0004519 | Endonuclease activity | 22 | 41 | 2.65 | 13 | 0.59 | 577.5 |
| 32 | GO:0009187 | Cyclic nucleotide metabolism | 10 | 60 | 2.88 | 7.5 | 0.55 | 598 |
| 33 | GO:0031252 | Leading edge | 18 | 50 | 2.51 | 20.5 | 0.54 | 603 |
| 34 | KEGG:rno00620 | Pyruvate metabolism | 11 | 64 | 2.65 | 13 | 0.46 | 655.5 |
| 35 | GO:0000287 | Magnesium ion binding | 78 | 37 | 2.51 | 20.5 | −0.45 | 659.5 |
| 36 | GO:0016776 | Phosphotransferase activity, phosphate group as acceptor | 14 | 36 | −0.2 | 676 | −1.91 | 13.5 |
| 37 | GO:0016567 | Protein ubiquitination | 59 | 29 | −0.18 | 685 | −1.75 | 22 |
| 38 | GO:0042995 | Cell projection | 63 | 40 | 2.95 | 5 | 0.35 | 705 |
| 39 | GO:0016627 | Oxidoreductase activity, acting on the CH–CH group of donors | 16 | 63 | 3.82 | 1 | 0.33 | 715 |
| 40 | GO:0004518 | Nuclease activity | 29 | 34 | 2.58 | 17 | 0.35 | 705 |
| 41 | KEGG:rno00071 | Fatty acid metabolism | 20 | 45 | 2.88 | 7.5 | 0.32 | 720 |
| 42 | GO:0008610 | Lipid biosynthesis | 61 | 41 | 2.65 | 13 | −0.32 | 720 |
| 43 | GO:0006631 | Fatty acid metabolism | 53 | 40 | 2.75 | 9.5 | −0.18 | 768.5 |
| 44 | GO:0006694 | Steroid biosynthesis | 28 | 46 | 2.46 | 25 | −0.16 | 773.5 |
| 45 | KEGG:rno00230 | Purine metabolism | 27 | 37 | 2.65 | 13 | −0.01 | 802.5 |

Microdissected cholinergic neurons (200) from the BS of five young and five aged F344 rats were used for microarray analysis on Agilent Rat Oligo arrays (22,000 sequences). GeneSpring (v. 7.2) was used to "globally" normalize sets of genes expressed in at least 18 of 20 channels, treating each channel as an independent sample. The normalized data were exported to *R* and missing values were imputed before running the SigPathway program. The gene sets were ranked according to the average of $NT_k$ and $NE_k$ statistics.

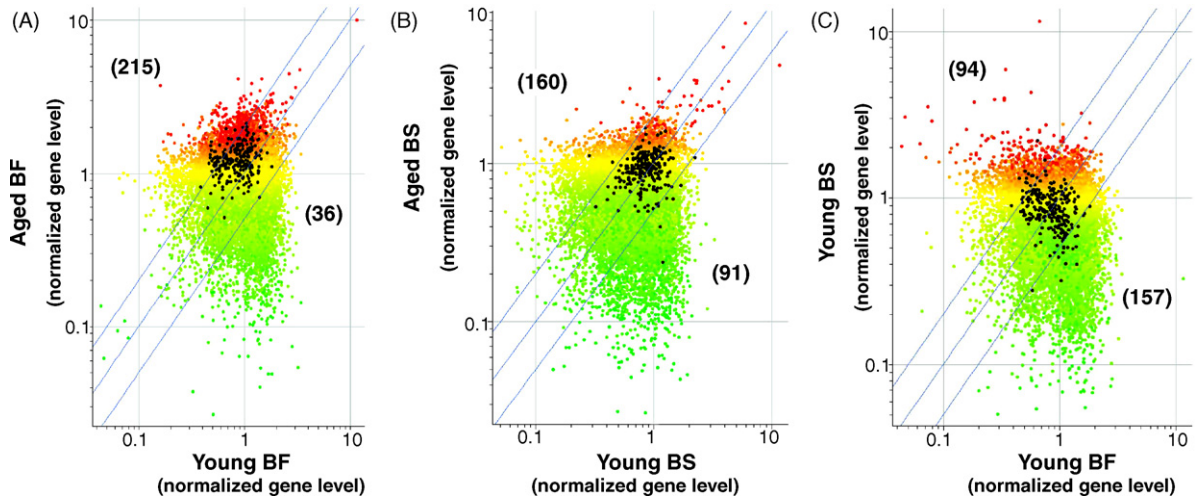


Fig. 5. Expression of a set of 251 metabolic genes in young and aged BF and BS cholinergic neurons. The SigPathway program was used to identify ontological sets of genes that were differently altered in expression level by the effects of age in BF and BS cholinergic populations. Thirteen (13) groups from the LOWESS normalized data in Table 1 and 18 groups in the globally normalized data in Table 2 were combined into a group of 251 general metabolic genes. The colored dots plot normalized expression levels ("1" indicates the mean level across all 20 channels) of genes that were present in at least 10 of 20 channels of the 10 microarrays. The warmer colors indicate higher levels (RED = up to five-fold or more over mean), while the cooler colors indicate expression levels below the mean (GREEN = down to one-fifth of the mean). Each plot in A, B or C is colorized according to the range of values for the phenotype plotted on the vertical axis. The central blue diagonal line represents equivalent expression for the two phenotypes plotted on the X and Y axes, while the two other blue diagonal lines indicate expression levels that are two-fold higher or lower. The black numbers in parentheses indicate those genes in the composite metabolic gene set that are above or below the line of equivalent expression.

this table the majority of the genes are more elevated by aging in the BF than in the BS (indicated by values greater than 50% under "Percent Up"). Genes associated with metabolic activity are contained in the multiple groups shown in Table 1 (groups 6, 14, 18, 19, 22, 27, 29, 30, 31, 33, 36 and 37). There were a total of 229 individual genes in these groups.

Tables 2 and 3 contain the SigPathway results for the BF and BS cholinergic groups, respectively, using the single channel, globally normalized data from this experiment. Over half of the groups in the list of gene ontologies for the BF contain genes involved in ATP/GTP synthesis (Table 1); 84 unique genes are contained in these groups. With all of these groups the large majority of their genes were upregulated in the aging BF. In contrast, the gene groups for the BS cholinergic population are primarily involved with signaling and plasticity, and both up and downregulation is evident (Table 2).

There are obvious qualitative similarities between the gene groupings for the microarray results processed either by LOWESS on the channel ratios or as globally normalized independent channels. Of the 84 metabolic genes in the metabolic gene sets in the BF single channel data, 62 are also in the set of 229 metabolic genes in the LOWESS processed data. The combination of the two gene sets results in 251 individual metabolic genes. Fig. 5A shows a scatterplot of these genes superimposed on the normalized single channel data for the BF (aged versus young). The majority (215) of these plot above the line of equivalent expression, with 36 below, indicating a strong bias towards upregulation of metabolic genes elicited by aging. For the aging BS there was also a bias towards upregulation of expression of these 251 genes, but it was much less pronounced (Fig. 5B). The plot of young BS versus young BF indicates that the majority of the metabolic genes are expressed at higher levels in the BF (Fig. 5C). The 251 metabolic genes represent a wide variety of biological functions (Table 4 ). Some examples include:

*glycolysis* (e.g., phosphofructokinase; hexokinase 1);
*glutathione metabolism* (e.g., glutathione peroxidase type 4; glutaredoxin 1);
*mitochondrial electron transport chain* (e.g., succinate dehydrogenase; cytochrome *c* oxidase);
*fatty acid metabolism* (e.g., acyl-Coenzyme A oxidase);
*proton transport and exchange* (e.g., ATP synthase subunits);
*water transport* (aquaporin 7);
*oxidation and reduction* (e.g., cytochrome P450 subunits; thioredoxins, peroxiredoxins, nucleoredoxin);
*metal ion transport* (e.g., $Na^+/K^+$ ATPase; $Ca^{2+}$ ATPase; solute carrier 9 $Na^+/H^+$ exchanger);
*translational and transcriptional regulation* (e.g., eukaryotic translation initiation factor 2 alpha kinase 3; hypoxia inducible factor 1; TATA box binding protein-like 1);
*the "salvage" DNA synthesis pathway* (hypoxanthine-guanine phosphoribosyltransferase);
*nitric oxide and carbon monoxide synthesis and signaling* (e.g., nitric oxide synthase type 2; heme oxygenase 2; biliverdin reductase A);
*maintenance of protein structure during synthesis in the endoplasmic reticulum* (prolyl 4-hydroxylase beta subunit);
*receptors and signaling* (prostaglandin I2 synthase, arginine vasopressin; neurotensin receptor type 2; gastric inhibitory

Table 4
Metabolic genes upregulated predominantly in aged BF cholinergic neurons

| Common | UniGene | Genbank | Description |
|---|---|---|---|
| Tpi1 | | NM_022922 | Triosephosphate isomerase 1 |
| TC525656 | | TC525656 | Unknown |
| Cyb5 | | NM_022245 | Cytochrome b-5 |
| Glrx1 | Rn.1484 | NM_022278 | Glutaredoxin 1 (thioltransferase) |
| U73859 | Rn.49623 | U73859 | Hexokinase type III |
| Atp5o | | NM_138883 | ATP synthase, $H^+$ transporting, mitochondrial F1 complex, O subunit |
| Atp6v1f | | NM_053884 | ATPase, $H^+$ transporting, V1 subunit F |
| Cycs | Rn.2202 | NM_012839 | Cytochrome *c*, somatic |
| Pfkl | | NM_013190 | Phosphofructokinase, liver, B-type |
| Cyp51 | Rn.107152 | NM_012941 | Cytochrome P450, subfamily 51 |
| Uqcrb | | XM_343225 | Similar to ubiquinol-cytochrome *c* reductase binding protein |
| Fhl1 | | BC061782 | Four and a half LIM domains 1 |
| Surf1 | | NM_172068 | Surfeit 1 |
| Cyb561 | | XM_221030 | Cytochrome b-561 (predicted) |
| Gaa | | NM_199118 | Glucosidase, alpha; acid (Pompe disease, glycogen storage disease type II) |
| Fh1 | | NM_017005 | Fumarate hydratase 1 |
| Cox4i2 | Rn.7214 | NM_053472 | Cytochrome *c* oxidase subunit IV isoform 2 |
| TC523783 | Rn.59092 | TC523783 | Q8R0Y3 (Q8R0Y3) Mtrr protein |
| Ndufb6 | Rn.104528 | A_43_P15698 | NADH dehydrogenase (ubiquinone) 1 beta subcomplex, 6 (predicted) |
| Nxn | Rn.105982 | XM_340857 | Nucleoredoxin (predicted) |
| Erbb2 | Rn.93966 | NM_017003 | v-erb-b2 erythroblastic leukemia viral oncogene homolog 2 (Erbb2) |
| Pgam1 | Rn.1383 | NM_053290 | Phosphoglycerate mutase 1 |
| Nos2 | Rn.10400 | NM_012611 | Nitric oxide synthase 2, inducible (Nos2) |
| Atp6v1a1 | Rn.1431 | TC535380 | Similar to ATPase, $H^+$ transporting, V1 subunit A, isoform 1 |
| Gpx6 | | NM_147165 | Glutathione peroxidase 6 |
| GAPDH | Rn.91450 | XM_574137 | Similar to Glyceraldehyde-3-phosphate dehydrogenase (GAPDH) |
| Prdx6 | | NM_053576 | Peroxiredoxin 6 |
| Cox6c | Rn.846 | NM_019360 | Cytochrome *c* oxidase, subunit Vic |
| Pgam2 | Rn.9738 | NM_017328 | Phosphoglycerate mutase 2 |
| Atp6v0c | | NM_130823 | ATPase, $H^+$ transporting, V0 subunit C |
| Atp1b3 | | NM_012913 | ATPase, $Na^+/K^+$ transporting, beta 3 polypeptide |
| Gpr37 | | NM_057201 | G protein-coupled receptor 37 |
| Pdcd8 | Rn.8124 | NM_031356 | Programmed cell death 8 |
| Eif2ak3 | | NM_031599 | Eukaryotic translation initiation factor 2 alpha kinase 3 |
| Avp | Rn.9976 | NM_016992 | Arginine vasopressin |
| TC554820 | | TC554820 | Unknown |
| Pygm | Rn.11238 | XM_342002 | Muscle glycogen phosphorylase |
| TC572408 | | TC572408 | Q71RR7 (Q71RR7) Guanylate kinase |
| Dnajc10 | | XM_215751 | DnaJ (Hsp40) homolog, subfamily C, member 10 (predicted) |
| Papss1 | | XM_215701 | Similar to ATP sulfurylase/APS kinase |
| COX-VIc-1 | | NM_173303 | Cytochrome *c* oxidase subunit VIc-1 |
| Blvra | Rn.9865 | NM_053850 | Biliverdin reductase A |
| TC521564 | | TC521564 | Q8IUE7 (Q8IUE7) STAMP1 |
| Aass | Rn.106953 | XM_231524 | Aminoadipate-semialdehyde synthase (predicted) |
| Acadl | | NM_012819 | Acetyl-coenzyme A dehydrogenase, long-chain |
| Gpx7 | Rn.4130 | XM_216473 | Similar to RIKEN cDNA 3110050F08 |
| Txndc7 | Rn.2685 | XM_576132 | Thioredoxin domain containing 7 |
| Ak1 | | NM_024349 | Adenylate kinase 1 |
| Txn | | NM_053800 | Thioredoxin |
| Ndufa5 | Rn.100240 | NM_012985 | NADH dehydrogenase (ubiquinone) 1 alpha subcomplex 5 |
| Gbe1 | Rn.104812 | XM_221747 | Glucan (1,4-alpha-), branching enzyme 1 (predicted) |
| Ntsr2 | Rn.127792 | NM_022695 | Neurotensin receptor 2 |
| Cyp21a1 | Rn.36545 | NM_057101 | Cytochrome P450, subfamily 21A, polypeptide 1 |
| Gipr | Rn.9676 | NM_012714 | Gastric inhibitory polypeptide receptor |
| Txnl1 | Rn.40430 | NM_080887 | Thioredoxin-like (32kD) |
| Pygl | | NM_022268 | Iver glycogen phosphorylase |
| Pdha1 | Rn.3655 | NM_001004072 | Pyruvate dehydrogenase E1 alpha 1 |
| Cox8a | | XM_574609 | Cytochrome *c* oxidase, subunit VIIIa |
| Qdpr | Rn.241 | NM_022390 | Quinoid dihydropteridine reductase |
| Nme1 | Rn.6236 | NM_138548 | Expressed in non-metastatic cells 1 |
| Atp5j | Rn.5790 | NM_053602 | ATP synthase, $H^+$ transporting, mitochondrial F0 complex, subunit F6 |
| Atf4 | | NM_024403 | Activating transcription factor 4 |
| Tnni2 | | NM_017185 | Troponin 1, type 2 |

Table 4 (*Continued*)

| Common | UniGene | Genbank | Description |
|---|---|---|---|
| Echs1 | Rn.6847 | NM_078623 | Enoyl Coenzyme A hydratase, short chain, 1, mitochondrial |
| Ppp1r2 | | NM_138823 | Protein phosphatase 1, regulatory (inhibitor) subunit 2 |
| Acads | Rn.1167 | NM_022512 | Acyl-coenzyme A dehydrogenase, short chain |
| Etfdh | | NM_198742 | Electron-transferring-flavoprotein dehydrogenase |
| Lao1 | Rn.81472 | XM_216521 | L-amino acid oxidase 1 (predicted) |
| Aldh3a1 | Rn.105627 | NM_031972 | Aldehyde dehydrogenase family 3, member A1 |
| TC559608 | | TC559608 | Unknown |
| Txn2 | Rn.55043 | NM_053331 | Thioredoxin 2 |
| Mdh1 | Rn.13492 | NM_033235 | Malate dehydrogenase 1, NAD (soluble) |
| Dmgdh | Rn.3646 | NM_139102 | Dimethylglycine dehydrogenase precursor |
| Coq7 | | NM_012785 | Demethyl-Q 7 |
| Atp1a2 | | NM_012505 | ATPase, $Na^+/K^+$ transporting, alpha 2 polypeptide |
| TC556774 | Rn.6389 | TC556774 | Unknown |
| Cyp4f2 | Rn.5722 | NM_019623 | Cytochrome P450, family 4, subfamily F, polypeptide 2 |
| TC557056 | | TC557056 | Unknown |
| Gpx4 | | NM_017165 | Glutathione peroxidase 4 |
| G6pc | Rn.10992 | NM_013098 | Glucose-6-phosphatase, catalytic |
| Akr1a1 | Rn.835 | NM_031000 | Aldo-keto reductase family 1, member A1 |
| Fmo1 | | NM_012792 | Flavin containing monooxygenase 1 |
| AA818664 | Rn.9756 | AA818664 | cDNA clone UI-R-A0-az-h-02-0-UI 3' similar to gb [AA818664] |
| Pcyox1 | | NM_145085 | Chloride ion pump-associated 55 kDa protein |
| Cyb561d1 | Rn.67979 | XM_342315 | Cytochrome b-561 domain containing 1 (predicted) |
| Bat3 | | NM_053609 | HLA-B-associated transcript 3 |
| Cybb | | NM_023965 | Cytochrome b-245, beta polypeptide |
| Txndc1 | Rn.123627 | XM_343076 | Similar to Txndc1 protein |
| AW532167 | | AW532167 | cDNA clone UI-R-C4-alj-b-07-0-UI |
| Adss2 | | XM_222946 | Adenylosuccinate synthetase 2, non-muscle (predicted) |
| P2rx4 | Rn.7176 | NM_031594 | Purinergic receptor P2X, ligand-gated ion channel, 4 |
| BF559350 | Rn.64648 | BF559350 | cDNA clone UI-R-E1-fb-f-12-0-UI |
| Slc37a4 | Rn.1592 | NM_031589 | Solute carrier family 37 (glycerol-6-phosphate transporter), member 4 |
| Atp8b1 | Rn.6957 | XM_214553 | ATPase, Class I, type 8B, member 1 (predicted) |
| Uqcrfs1 | | XM_214457 | Similar to RIKEN cDNA 4430402G14 |
| Atp1b2 | Rn.10624 | NM_012507 | ATPase, $Na^+/K^+$ transporting, beta 2 polypeptide |
| Aldoc | Rn.11211 | NM_012497 | Aldolase C, fructose-biphosphate |
| TC553514 | Rn.14673 | TC553514 | Cytochrome b561 |
| Slc30a5 | Rn.16711 | XM_226722 | Solute carrier family 30 (zinc transporter), member 5 (predicted) |
| Aqp7 | | NM_019157 | Aquaporin 7 |
| Tyki | | XM_234017 | Thymidylate kinase family LPS-inducible member (predicted) |
| Atp6v0e | | NM_053578 | ATPase, $H^+$ transporting, V0 subunit |
| Limk2 | | NM_024135 | LIM motif-containing protein kinase 2 |
| Cox5a | | NM_145783 | Cytochrome *c* oxidase, subunit Va |
| Atp5a1 | | NM_023093 | ATP synthase, $H^+$ transporting, mitochondrial F1 complex, alpha subunit, isoform 1 |
| Ndufb9 | | XM_216929 | NADH dehydrogenase (ubiquinone) 1 beta subcomplex, 9 (predicted) |
| Slc9a5 | Rn.24105 | NM_138858 | Solute carrier family 9 (sodium/hydrogen exchanger), isoform 5 |
| Sdhd | | NM_198788 | Succinate dehydrogenase complex, subunit D, integral membrane protein |
| Aldh2 | Rn.101781 | NM_032416 | Aldehyde dehydrogenase 2 |
| Nme3 | Rn.8785 | NM_053507 | Non-metastatic cells 3, protein expressed in |
| Abcb11 | | NM_031760 | ATP-binding cassette, sub-family B (MDR/TAP), member 11 |
| AA944202 | Rn.4445 | AA944202 | EST199701 Normalized rat embryo |
| Lcmt2 | Rn.17983 | NM_001011956 | Leucine carboxyl methyltransferase 2 (predicted) |
| Gpd2 | | NM_012736 | Glycerol-3-phosphate dehydrogenase 2 |
| Blvrb | | XM_214823 | Biliverdin reductase B (flavin reductase (NADPH)) (predicted) |
| CB546986 | Rn.2465 | CB546986 | cDNA clone srcs1-00110-f6 |
| Nme6 | | XM_343488 | Expressed in non-metastatic cells 6, protein (nucleoside diphosphate kinase) |
| Bsn | | NM_019146 | Bassoon |
| Mgst3 | | XM_213943 | Microsomal glutathione S-transferase 3 (predicted) |
| Paics | Rn.3015 | NM_080910 | Phosphoribosylaminoribosylaminoimidazole succinocarboxamide synthetase |
| Mth1 | Rn.10669 | NM_057120 | Nudix (nucleoside diphosphate linked moiety X)-type motif 1 |
| Txndc4 | | XM_216396 | Similar to thioredoxin domain containing 4; ER resident protein 44kDa |
| Gaa | Rn.60475 | NM_199118 | Glucosidase, alpha; acid (Pompe disease, glycogen storage disease type II) |
| Ech1 | | NM_022594 | Enoyl coenzyme A hydratase 1, peroxisomal |
| TC519886 | Rn.123577 | TC519886 | Phosphoribosylformylglycinamidine synthase |
| Atp5f1 | | NM_134365 | ATP synthase, $H^+$ transporting, mitochondrial F0 complex, subunit b, isoform 1 |
| AA899832 | | AA899832 | cDNA clone UI-R-E0-cq-f-04-0-UI |

Table 4 (*Continued*)

| Common | UniGene | Genbank | Description |
|---|---|---|---|
| Cyp11a1 | Rn.1401 | NM_017286 | Cytochrome P450, family 11, subfamily a, polypeptide 1 |
| Pgk1 | Rn.108127 | M31788 | Rat X-chromosome linked phosphoglycerate kinase |
| Atp5g1 | Rn.3357 | NM_017311 | ATP synthase, $H^+$ transporting, mitochondrial F0 complex, subunit c (subunit 9) |
| TC518963 | Rn.4016 | TC518963 | Phosphatase inhibitor-2 |
| CB547534 | Rn.47804 | CB547534 | cDNA clone trpa3-00003-a1 |
| Tbpl1 | Rn.25148 | XM_214744 | TATA box binding protein-like 1 (predicted) |
| Tat | | NM_012668 | Tyrosine aminotransferase |
| Ivd | | NM_012592 | Isovaleryl coenzyme A dehydrogenase |
| TC553253 | | TC553253 | Q8WUC4 (Q8WUC4) ACADSB protein (Fragment) |
| RGD1311345 | | XM_341483 | Similar to CG9752-PA (predicted) |
| Ppp1cb | Rn.39034 | NM_013065 | Protein phosphatase 1, catalytic subunit, beta isoform |
| Mor1 | Rn.1011 | X04240 | Mitochondrial malate dehydrogenase |
| Hif1a | Rn.10852 | NM_024359 | Hypoxia inducible factor 1, alpha subunit |
| Ndufb9 | Rn.22045 | XM_216929 | NADH dehydrogenase (ubiquinone) 1 beta subcomplex, 9 (predicted) |
| Prdx1 | Rn.2845 | NM_057114 | Peroxiredoxin 1 |
| Ndufs8 | | XM_215197 | NADH dehydrogenase (ubiquinone) Fe-S protein 8 (predicted) |
| Treh | | XM_576400 | Similar to RCK |
| TC522257 | | TC522257 | Unknown |
| Ppp1r1a | Rn.9756 | NM_022676 | Protein phosphatase 1, regulatory (inhibitor) subunit 1A |
| Ndufb5 | | XM_215544 | NADH dehydrogenase (ubiquinone) 1 beta subcomplex, 5 (predicted) |
| Atp6ap1 | Rn.93045 | NM_031785 | ATPase, $H^+$ transporting, lysosomal (vacuolar proton pump), subunit 1 |
| Txnl2 | | NM_032614 | Thioredoxin-like 2 |
| Gys2 | Rn.2906 | NM_013089 | Glycogen synthase 2 |
| Ndufb4 | | XM_213619 | NADH dehydrogenase (ubiquinone) 1 beta subcomplex, 4, 15kDa (predicted) |
| Aldh9a1 | Rn.98155 | NM_022273 | Aldehyde dehydrogenase family 9, subfamily A1 |
| MGC72942 | | NM_212516 | Similar to CG6105-PA |
| Uqcrh | | NM_001009480 | Ubiquinol-cytochrome *c* reductase hinge protein (predicted) |
| Acox1 | Rn.31796 | NM_017340 | Acyl-Coenzyme A oxidase 1, palmitoyl |
| Tpo | Rn.91199 | NM_019353 | Thyroid peroxidase |
| Aldh1a2 | | NM_053896 | Aldehyde dehydrogenase family 1, subfamily A2 |
| Pc | | NM_012744 | Pyruvate carboxylase |
| Cyp2d22 | Rn.26060 | NM_138515 | Cytochrome P450, family 2, subfamily d, polypeptide 22 |
| Sdhc | Rn.1698 | NM_001005534 | Succinate dehydrogenase complex, subunit C |
| Cyp2d26 | | NM_012730 | Cytochrome P450, family 2, subfamily d, polypeptide 26 |
| Sqle | Rn.33239 | NM_017136 | Squalene epoxidase |
| Txndc5 | | XM_225257 | Thioredoxin domain containing 5 (predicted) |
| Mutyh | Rn.44045 | NM_133316 | MutY homolog (E. coli) |
| Atp5i | Rn.66347 | NM_080481 | ATP synthase, $H^+$ transporting, mitochondrial F0 complex, subunit e |
| Suclg1 | | NM_053752 | Succinate-CoA ligase, GDP-forming, alpha subunit |
| Atp1a3 | Rn.87329 | NM_012506 | ATPase, $Na^+/K^+$ transporting, alpha 3 polypeptide |
| Atp6v0b | Rn.19803 | XM_216510 | ATPase, $H^+$ transporting, V0 subunit B (predicted) |
| Pkm2 | Rn.1556 | NM_053297 | Pyruvate kinase, muscle |
| TC553457 | Rn.17175 | TC553457 | Glutaredoxin 2 |
| Pfkm | | NM_031715 | Phosphofructokinase, muscle |
| Atp5h | Rn.80 | NM_019383 | ATP synthase, $H^+$ transporting, mitochondrial F0 complex, subunit d |
| Ndufb2 | Rn.18013 | | NADH dehydrogenase (ubiquinone) 1 beta subcomplex, 2 (predicted) |
| TC536567 | | TC536567 | Unknown |
| Ldhb | Rn.1785 | NM_012595 | Lactate dehydrogenase B |
| Hk1 | Rn.11017 | NM_012734 | Hexokinase 1 |
| Ppp1r3c | Rn.47439 | NM_001012072 | Protein phosphatase 1, regulatory (inhibitor) subunit 3C (predicted) |
| Atp5g2 | | NM_133556 | ATP synthase, $H^+$ transporting, mitochondrial F0 complex, subunit c isoform 2 |
| Me1 | | M30596 | Cytosolic malic enzyme |
| Slc9a1 | | NM_012652 | Solute carrier family 9, member 1 |
| Atp5c1 | | NM_053825 | ATP synthase, $H^+$ transporting, mitochondrial F1 complex, gamma polypeptide 1 |
| PDSW | Rn.2867 | XM_1059290.1 | Similar to NADH-ubiquinone oxidoreductase PDSW subunit |
| TC535339 | Rn.66581 | TC535339 | Citrate synthase |
| Vgf | Rn.9704 | NM_030997 | VGF nerve growth factor inducible |
| Slc25a3 | | NM_139100 | Solute carrier family 25 (mito carrier; adenine nucleotide translocator), member 3 |
| Rnf7 | Rn.2768 | XM_217235 | Ring finger protein 7 (predicted) |
| Ndufa6 | | XM_235518 | NADH dehydrogenase (ubiquinone) 1 alpha subcomplex, 6 (B14) (predicted) |
| Cox6a2 | | NM_012812 | Cytochrome *c* oxidase, subunit VIa, polypeptide 2 |
| Kif9 | | XM_236648 | Kinesin family member 9 (predicted) |
| TC534654 | Rn.105893 | TC534654 | Inner membrane protein OXA1L, mitochondrial precursor |
| TC518177 | Rn.35696 | TC518177 | BC011467 protein |

Table 4 (*Continued*)

| Common | UniGene | Genbank | Description |
|---|---|---|---|
| Atp2b3 | | XM_343839 | ATPase, $Ca^{2+}$ transporting, plasma membrane 3 |
| Idh3g | Rn.2837 | NM_031551 | Isocitrate dehydrogenase 3, gamma |
| Ppp1r3c | Rn.47439 | NM_001012072 | Protein phosphatase 1, regulatory (inhibitor) subunit 3C (predicted) |
| Atp6v1f | Rn.6167 | NM_053884 | ATPase, $H^+$ transporting, V1 subunit F |
| Pdcl | Rn.51153 | NM_022247 | phosducin-like |
| Idh3g | | NM_031551 | Isocitrate dehydrogenase 3, gamma |
| Pqlc1 | | NM_001013189 | PQ loop repeat containing 1 (predicted) |
| Cox7a3 | Rn.1745 | NM_022503 | Cytochrome *c* oxidase, subunit 7a 3 |
| Nme2 | | NM_031833 | Expressed in non-metastatic cells 2 |
| Atp5e | | NM_139099 | ATP synthase, $H^+$ transporting, mitochondrial F1 complex, epsilon subunit |
| Cox5b | Rn.6686 | NM_053586 | Cytochrome *c* oxidase subunit Vb |
| Atp13a | Rn.3697 | XM_214310 | ATPase type 13A (predicted) |
| Gsto1 | Rn.25166 | XM_342062 | Glutathione *S*-transferase omega 1 |
| Por | Rn.11359 | NM_031576 | P450 (cytochrome) oxidoreductase |
| Tyki | Rn.100440 | XM_234017 | Thymidylate kinase family LPS-inducible member (predicted) |
| Sdhb | Rn.3902 | XM_216558 | Succinate dehydrogenase complex, subunit B, iron sulfur (Ip) (predicted) |
| Sdha | | NM_130428 | Succinate dehydrogenase complex, subunit A, flavoprotein (Fp) |
| Pck2 | Rn.59912 | XM_341319 | Similar to RIKEN cDNA 9130022B02 |
| AW917082 | Rn.100240 | AW917082 | cDNA clone RGIDZ08 |
| G6pdx | Rn.11040 | NM_017006 | Glucose-6-phosphate dehydrogenase |
| Cyp51 | | NM_012941 | Cytochrome P450, subfamily 51 |
| Prdx2 | Rn.2511 | NM_017169 | Peroxiredoxin 2 |
| Dutp | Rn.6102 | NM_053592 | Deoxyuridine triphosphatase |
| Cdo1 | | NM_052809 | Cytosolic cysteine dioxygenase 1 |
| Ndufb3 | | XM_217400 | NADH dehydrogenase (ubiquinone) 1 beta subcomplex 3 (predicted) |
| Acadvl | | NM_012891 | Acyl-Coenzyme A dehydrogenase, very long chain |
| Srd5a2 | Rn.9938 | NM_022711 | Steroid 5-alpha-reductase 2 |
| Ndufv2 | | NM_031064 | NADH dehydrogenase (ubiquinone) flavoprotein 2 |
| Gad1 | Rn.91245 | NM_017007 | Glutamate decarboxylase 1 |
| Cyp51 | | NM_012941 | Cytochrome P450, subfamily 51 |
| RGD1309462 | | NM_001009697 | Similar to RIKEN cDNA 2310020P08 (predicted) |
| Atp5c1 | | NM_053825 | ATP synthase, $H^+$ transporting, mitochondrial F1 complex, gamma polypeptide 1 |
| TC553106 | Rn.2517 | TC553106 | LIM domain transcription factor LMO4 (LIM-only protein 4) |
| Adss2 | Rn.9047 | XM_222946 | Adenylosuccinate synthetase 2, non=muscle (predicted) |
| XM_574642 | | XM_574642 | Similar to frataxin |
| Degs | Rn.34792 | NM_053323 | Degenerative spermatocyte homolog (Drosophila) |
| Qscn6 | Rn.44920 | NM_053431 | quiescin Q6 |
| Acadl | Rn.174 | NM_012819 | Acetyl-Coenzyme A dehydrogenase, long-chain |
| Aldoa | | NM_012495 | Aldolase A |
| Cyp27b1 | Rn.10847 | NM_053763 | Cytochrome P450, family 27, subfamily b, polypeptide 1 |
| Mgat2 | Rn.2342 | NM_053604 | Alpha-1,6-mannosyl-glycoprotein 2-beta-N-acetylglucosaminyltransferase |
| Atp2a2 | | NM_017290 | ATPase, $Ca^{2+}$ transporting, cardiac muscle, slow twitch 2 |
| TC521307 | | TC521307 | Unknown |
| Oxa1l | Rn.105893 | XM_214182 | Similar to Cytochrome oxidase biogenesis protein OXA1 |
| Hprt | Rn.47 | M86443 | Hypoxanthine-guanine phosporibosyltransferase |
| Prdx2 | | NM_017169 | peroxiredoxin 2 |
| Gldc | Rn.17101 | XM_219785 | Glycine dehydrogenase (decarboxylating |
| TC524952 | | TC524952 | NADPH-dependent FMN and FAD containing oxidoreductase |
| Cyp2d26 | Rn.91355 | NM_012730 | Cytochrome P450, family 2, subfamily d, polypeptide 26 |
| RGD1305413 | Rn.104592 | XM_342199 | Similar to FLJ40243 protein (predicted) |
| Ptgis | Rn.73051 | NM_031557 | Prostaglandin I2 (prostacyclin) synthase |
| Atp2c1 | Rn.5805 | NM_131907 | ATPase, $Ca^{2+}$-sequestering |
| Dld | Rn.86962 | XM_216682 | Similar to dihydrolipoamide dehydrogenase |
| Cyp8b1 | | NM_031241 | Cytochrome P450, family 8, subfamily b, polypeptide 1 |
| TC540683 | | TC540683 | EbiP338 |
| Acad9 | | XM_574921 | Acyl-Coenzyme A dehydrogenase family, member 9 |
| Wfs1 | Rn.16015 | NM_031823 | Wolfram syndrome 1 |
| Hmox2 | Rn.10241 | NM_024387 | Heme oxygenase (decycling) 2 |
| P4hb | Rn.4234 | NM_012998 | Prolyl 4-hydroxylase, beta polypeptide |
| Mll | Rn.62341 | XM_236194 | Myeloid/lymphoid or mixed-lineage leukemia |

Ontological groupings with metabolic genes resulting from SigPathway analysis of BF age effects of both LOWESS and single channel data were combined and 251 unique genes were identified.

polypeptide receptor; VGF nerve growth factor inducible protein).

This complexity suggests that aging has led to the activation of numerous signaling pathways in BF cholinergic neurons.

### 3.4. Validation of differential expression of indicator genes

Because the amount of total RNA obtained from 200 neurons was extremely limited and was used for amplification, it was necessary to use aRNA produced from the second stage of the T7 amplification for validation. The genes we chose to validate are all members of the metabolism-related ontologies that were upregulated to a greater degree in aged BF than in aged BS. However, their "fold" upregulation in the microarray data was in most cases two-fold or less. While the statistical approach of SigPathway is powerful enough in identifying these genes within ontological groups, the variance intrinsic to qRT-PCR makes it extremely difficult to attain statistical reliance when validating gene level differences on this order. There was also substantial biological variance; i.e., gene levels between individuals could be several-fold different.

Despite these limitations we found that *as a composite* the qRT-PCR data for these nine genes strongly supported the microarray data. The aged/young ratios were calculated from the microarray data (from single channel data) and plotted against the corresponding ratios calculated from qRT-PCR data (Fig. 6). The correlation coefficient for the combined data ($R^2 = 0.0.627$; $R = 0.792$) was highly significant ($p < 0.001$). The correlations for individual brain regions were also significant (BF: $R^2 = 0.612$, $R = 0.782$, $p < 0.02$; BS: $R^2 = 0.629$, $R = 0.793$, $p < 0.02$). We also plotted the qRT-PCR data versus the LOWESS-normalized microarray data, and also obtained a significant correlation ($R^2 = 0.558$, $R = 0.747$, $p < 0.001$; not shown). These correlations are strong evidence that the microarray data are valid results. One caveat to this validation is that, because of the limiting amount of source mRNA, we were not able to perform qRT-PCR on unamplified material. Indeed, the most convincing validation would be achieved by confirming these mRNA alterations with a completely independent set of subjects either by in situ hybridization histochemistry or qRT-PCR. This would be a priority in the next phase of this project.

### 3.5. Evidence for activation of transcription factor GABPα

A type of "validation" for the mRNA alterations observed on our microarrays can be accomplished independently at the protein level if the activation a transcriptional system known to be involved in some or all of the alterations can be demonstrated. GABPα/β in rodents is equivalent to human "nuclear respiratory factors" NRF-1/NRF-2. These factors regulate the transcription of nuclear genes the mRNAs of

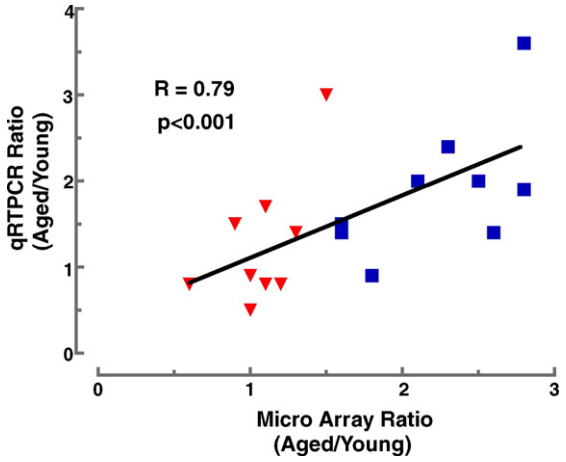


Fig. 6. Correlations between microarray data and RT-PCR data for nine genes in microdissected cholinergic neurons in young and aged F344 rats. Double-stranded DNA from the second stage of T7-amplification of mRNA from 200 cholinergic neurons microdissected from the BF and BS of five young and five aged F344 rats was used to generate aRNA ("amplified RNA"). The aRNA was reverse transcribed and the real-time PCR was performed for nine candidate metabolic genes and GAPDH. Analyses for each gene and sample was repeated three to six times, as was the reference gene (GAPDH), and the abundance of genes calculated as described in Section 2. The ratio of aged gene level to young gene level was calculated from the qRT-PCR data and plotted against the same ratio calculated from the globally normalized microarray data. Red inverted triangles represent the ratios of the nine genes in the BS aged/young data, and the blue squares are the ratios of the nine genes in the BF aged/young data. Note that ratios for the BF genes plot to the right of the BS genes, indicating age-induced upregulation predominating in the BF.

which will be translated in the cytosol and the proteins produced will be imported into mitochondria (Scarpulla, 2006). The great majority of proteins in the mitochondria are transcribed from nuclear-encoded genes. GABPα exists in a cytosolic reservoir and translocates to the nucleus to elicit increased expression of mitochondrial proteins (Yang et al., 2004). This occurs in neurons upon depolarization (Yang et al., 2006). The SigPathway results clearly indicate that many mitochondrial genes are increased in expression in the aged BF, suggesting a coordinated transcriptional activation. We performed a dual immunocytochemical characterization of both the basal forebrain and pontine cholinergic groups from three of the young and three of the aged subjects that were used for microdissection, in which we localized GABPα-like reactivity (blue deposits) within cholinergic neurons visualized with an antibody to choline acetyltransferase (ChAT; brown deposits). A semi-quantitative analysis was performed "blinded", in which the level of nuclear GABPα staining was judged on a scale from zero (0) to five (5). Fig. 7 shows color photomicrographs of typical neuronal fields in the BF and BS of young and aged subjects. The level of nuclear (blue) GABPα in (brown) ChAT-positive perikarya varied widely in both brain regions. The constitutive nature of this transcriptional system is evidenced by the present of nuclear GABPα in virtually all cholinergic neurons, as well as non-cholinergic cells. In this figure, many of the cholinergic neurons are

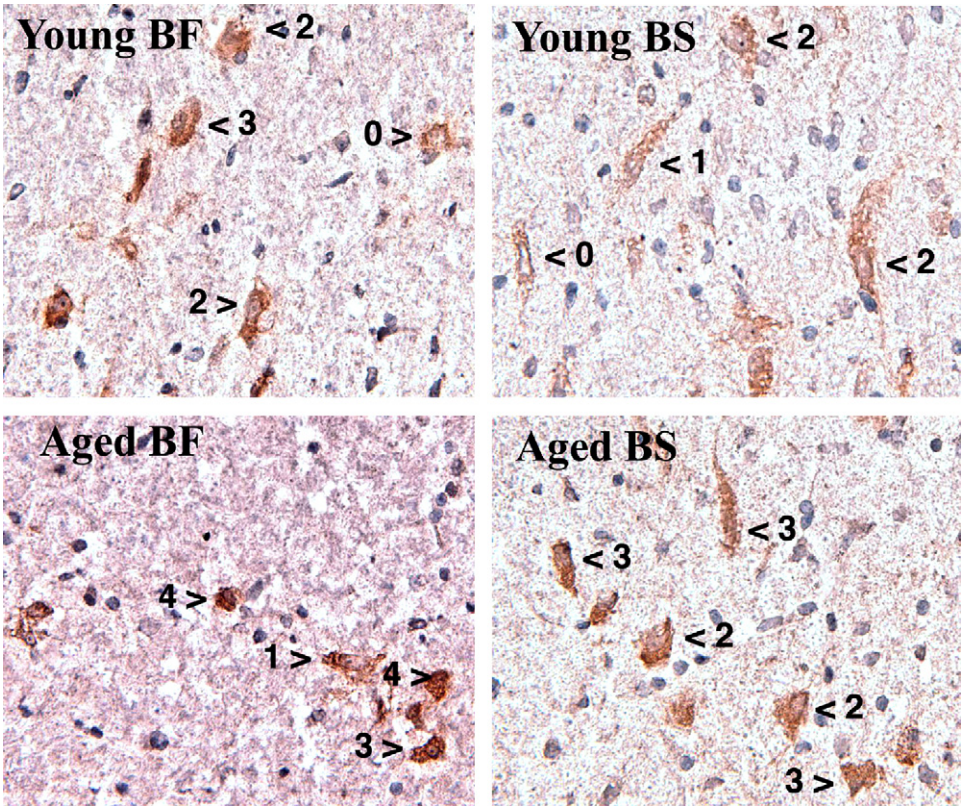


Fig. 7. Immunostaining for a nuclear-encoded transcription factor (GABPα) for mitochondrial genes in BF and BS cholinergic (ChAT-positive) neuron in young and aged F344 rats. Three young and three aged subjects (a subset of the rats used for microarray analyses) were used. Choline acetyltransferase was visualized by a peroxidase reaction with diaminobenzidine as substrate (brown deposits), and GABPα was visualized by nickel-enhancement of diaminobenzidine (blue deposits). The numbers in the plots indicate examples of observer grading of expression level of GABPα reactivity (0 = none visible, to 5 = strongest).

labeled with numbers from 0 to 5, according to the assessed level of nuclear GABPα, to demonstrate the amount of variation present. Several hundred cholinergic neurons were assessed in both BF and BS in all six subjects, and weighted averages of GABPα staining intensities were calculated (Table 5). Despite the variability of gene expression that exists in these populations, statistically reliable increases in nuclear GABPα were demonstrated in the aging BF (+107%; $p < -0.05$) and aging BS (+40%; $p < 0.02$). These findings are consistent with the hypothesis that aging induces expression of mitochondrial genes, with more effect on the BF group.

One the genes controlled by GABPα/β is mitochondrial transcription factor A (Piantadosi and Suliman, 2006). This factor is involved in the transcription of genes within the mitochondrion. Fig. 3 shows that the mRNA for this gene is increased in the aged BF (average = 2.5, $n = 5$) and decreased in the aged BS (average = 0.6, $n = 5$). These changes in levels of transcription factor A were in agreement with the qRT-PCR

Table 5
Nuclear levels of GABPα in BF and BS cholinergic neurons of young and aged F344 rats

| | 0[a] | 1[a] | 2[a] | 3[a] | 4[a] | 5[a] | Weighted average (±S.E.) |
|---|---|---|---|---|---|---|---|
| % of Total GABPα immunostained nuclei in ChAT-positive neurons (number counted) | | | | | | | |
| Young BF ($n = 3$) | 12.7 (83) | 31.2 (204) | 32.3 (211) | 19.5 (127) | 4.3 (28) | 0 (0) | 0.978 ± 0.294 |
| Aged BF ($n = 3$) | 6.6 (48) | 23.9 (175) | 38.8 (284) | 22.8 (167) | 7.9 (58) | 0 (0) | 2.027 ± 0.159 ($p < 0.05$) |
| Young BS ($n = 3$) | 19.9 (129) | 67.0 (435) | 12.8 (83) | 0.3 (2) | 0 (0) | 0 (0) | 0.938 ± 0.065 |
| Aged BS ($n = 3$) | 20.0 (182) | 37.0 (328) | 33.9 (301) | 8.2 (73) | 0.3 (3) | 0 (0) | 1.31 ± 0.0651 ($p < 0.01$) |

A two-color immunostaining protocol was used (see Fig. 6). Sections (6–12) through the MS/DB and upper pontine regions from three young and three aged F344 rats were processed in the same experiment and the quantitations were performed by a "blinded" observer. The staining level was graded from "0" (no discernible nuclear deposit) to "5" (intense GABPα immunoreaction deposits). The numbers of ChAT-GABPα stained neurons quantitated are shown in parentheses, along with the percentage of the total, for each phenotype, combining the data from three individual subjects. However, the weighted averages of nuclear GABPα staining levels were calculated for individual subjects. The averages ± standard errors for each phenotype are shown in the column at far right. There was a statistically reliable ($p < 0.05$) increase (+107%) in the aged BF, as compared to young BF. There was also a significant ($p < 0.01$) increase (+39%) in the aged BS, as compared to the young BS (Student's *t*-test).

[a] Staining level.

experiments, in which we observed a BF aged/young ratio of 2.0 and a BS aged/young ratio of 0.8. Differences in the level of mRNA for mitochondrial transcription factor A, averaged across individual young and aged animals were not statistically reliable ($p > 0.05$) in either the microarray data or the qRT-PCR data, but this was expected given the biological and technical variability, and the modest changes in mRNA levels.

## 4. Discussion

In this study, we have demonstrated that aging elicits increased expression of genes involved in energy production in cholinergic neurons, more profoundly in basal forebrain than in the PPN/LDTN located in the pontine reticular formation. For most metabolic genes, the maximal degree of upregulation was on the order of a modest 50–100% over levels in the young brain. Standard statistical methods evaluating individual genes would be of marginal use in revealing these changes in a reliable or convincing manner. However, when ontological groupings of genes were assessed using SigPathway, their coordinated upregulation was readily demonstrated. Many of the genes upregulated in the BF encode mitochondrial proteins, which are in large part regulated by the GA-binding protein transcriptional system. The involvement of GABPα/β in mediating the age effects was indicated by the findings of increased nuclear levels of GABPα-like immunoreactivity, to a greater degree in the BF cholinergic population.

The development of methods of amplifying mRNA in total RNA extracts from small numbers of cells, coupled with the commercial availability of machines (Arcturus, Leica), make it possible to collect individual cells and perform genome-wide studies of gene expression. Most of the commercially available protocols and kits use some variation on the T7 RNA polymerase based method initially established by Eberwine and colleagues (Van Gelder et al., 1990). Although powerful, this method is difficult to apply to single cells; however, with the commercial microdissecting machines, a few hundred cells can be collected in a reasonable timeframe, and this number provides enough mRNA to reliably amplify with the T7 method. Extensive studies of the T7 method have established that it amplifies reliably and with an acceptably low level of skewing. The 3′ bias inherent in the method is offset by the use of microarrays configured with probes from this region of the coding sequence.

Methods of analyzing data from microarray studies have, and continue to, evolve. From a classical statistical perspective, a good deal of attention has been given to the problem of false positives. If microarray data were truly random, there would be an unacceptably high proportion of false positives, when analyzed with standard parametric approaches. However, the levels of genes in a biological setting are not random events, but rather consequences of activities in interconnected and branching signaling pathways. Many genes are regulated coordinately, as they are controlled by one or a few major transcriptional systems. Moreover, the expression levels of less obviously related genes can exhibit interdependencies resulting from multiple interactions between pathways at multiple levels. Thus, a classical statistical approach to microarray analysis, while conservative, may not be justified.

An appealing microarray analytical approach, called "pathway analysis", makes use of the fact that genes involved in a common function and/or participating in a common signaling pathway may be coordinately regulated. Extensive classification systems for most of the known genes already exist (e.g., GenMAPP, Gene Ontology). These classifications can be used in microarray analysis to determine whether groups of genes related to particular biological functions are regulated in the same direction of expression. This turns out to be true for many biological systems of interest, and the fact that related genes are regulated together provides considerable mechanistic insight. The combination of genes into biological groups also gives statistical power. If differentially expressed genes are examined individually with conventional parametric methods, greater degrees of change are usually needed to obtain acceptably reliable results. Moreover, sorting lists of such genes according to degree of expression change or degree of statistical significance usually produces a sequence of genes in no particular order of biological function or relatedness. It becomes especially difficult to identify the global patterns that occur with a large number of genes. Many genes of interest in a study of a biological system may exhibit relatively small degrees of change or significance, and may not appear near the top of the gene list, which is often the intuitive focus of interest. By considering groups of genes, we are able to detect coordinated changes even when changes in individual gene levels are modest and/or statistically unreliable. In the most commonly used form of pathway analysis, a hard threshold is used to divide the gene list into those that are differentially expressed and those that are not, resulting in loss of information. The SigPathway algorithm we used considers the continuum in the gene list and applies statistically rigorous criteria to discover the significant gene sets.

Our finding of age-induced metabolic gene upregulation predominating in the BF cholinergic group raises a number of provocative questions regarding the effects of normal aging as well as the responses of this group of neurons in age-related human diseases. Cognitive decline is a consequence for a cohort of aged subjects in "normal aging". In a model of aging in Long-Evans rats, we have shown that spatial learning deficits are associated with elevation of markers of oxidative stress (Nicolle et al., 2001). In this same model, a small loss of BF cholinergic neurons occurs, although this loss does not relate strongly to cognitive status (Baskerville et al., 2007). Humans also exhibit cognitive decline and elevated brain oxidative stress in normal aging (Foster, 2006). One interpretation of our data is that metabolic gene upregulation is a normal consequence of aging in the BF system; that is, it is "adaptive". While the elevated expression of mitochondrial genes could suggest elevated production of free radicals, and

consequently vulnerability, the degree of gene upregulation is fairly modest; it is conceivable that free radical elevation is also modest and sufficiently handled by cellular antioxidant systems. Thus, one implication of our findings is that this neuronal system must elevate metabolism to sustain its functions in the aged brain.

In this view, successful aging of the brain occurs by changing cellular and multi-cellular (circuitry) organization so that behavioral demands continue to be supported. An outstanding study that supports this view is one accomplished with human subjects by McIntosh and colleagues (Della-Maggiore et al., 2000). Young and aged subjects were trained to perform a cognitive task to equivalent levels, then fMRI was used to map the distribution of brain blood flow inferred from oxygen utilization, a surrogate indicator of neural activities supporting the performance of the task. Elegant methods of pathway analysis were used to infer the strengths of connectivity between those brain regions supporting the task. The startling finding was that young and aged subjects used the circuitry differently, implying that the aged brain finds ways to adapt to stresses placed upon it over the years, to continue functioning at a level equivalent to younger brains.

The major stressor in aging is probably oxidative stress and there are many cellular mechanisms of adaptation to its effects. A recent study demonstrated that, in normal human brain aging beginning about age 40, plasticity genes decline in expression and survival genes increase in level; oxidative damage to promoter regions appears to explain this (Lu et al., 2004). Thus, in the absence of disease, there are major effects of cumulative oxidative stress on brain gene expression. Our molecular profiling of two cholinergic neuronal systems in the aged F344 rat brain in the current study suggests that even within a particular neurotransmitter phenotype a population can exhibit *different* reactions to age-related stressors according to brain region. This infers that anatomy and function are major influences on how neurons react to aging: i.e., the physiological functions supported by the BF population somehow configures the overall gene expression regulatory system. In this rodent model, where there is no amyloid deposition, some other age-related aspect of the cortex, perhaps related to the elevation of oxidative stress (Nicolle et al., 2001), may lead to a metabolic upregulation in the BF. These cholinergic neurons have extensive projections to the entire telencephalon, to essentially all anatomic layers. While some of the connections are synaptic, there is evidence for non-synaptic or "volume" transmission as well (reviewed in McKinney et al., 2003). The released acetylcholine serves modulatory functions; extensive studies have shown that sensory input to cortical circuitry is potentiated by this acetylcholine. For example, direct electrical stimulation of the BF activates the cortical EEG (Lo Conte et al., 1982) and rapidly induces associative memory (Miasnikov et al., 2006). The level of activity in the basal forebrain cholinergic population is probably under the control of multiple sensory-related inputs and by stimuli related to global levels of brain activity ("brain state"). Additionally, there is likely to be some degree of "feedback" from cortical regions via projections from cortex to the BF. The oxidatively stressed aged cortex may experience a decrease in responsiveness to acetylcholine and compensate by demanding more input from the cholinergic population. This may cause increased firing rates or other physiological changes in the BF neurons, leading to signaling cascades that increase mitochondrial activity and/or content. Consistent with this idea is the fact that activation of neurons (Yang et al., 2006) or increased cellular energy demand (Ongwijitwat et al., 2006) is associated with increased gene induction by nuclear respiratory factors. Besides direct activation of BF neurons by cortical projections, another way the cortex might cause changes in BF cholinergic neurons could relate to the dependence of the latter on cortical neurotrophins. It is known that the neurotrophin BDNF is a regulator of the expression of mitochondrial respiratory coupling in neurons (Markham et al., 2004). An alteration in neurotrophin production or its efficacy might occur with aging, and this might alter the metabolic state of the BF population.

An alternative hypothesis regarding our findings of elevated metabolism of BF cholinergic neurons is that this may be a precursor to degeneration. Presumably, increased metabolic activity is accompanied by increases in free radical production, and this might combine with disease pathology to cause selective vulnerability. In the case of AD, the selective degeneration of the BF might be a partial consequence of aberrant metabolism of the amyloid precursor protein system. Most BF projections are to regions that become laden with amyloid deposits in AD, while most BS projections are to regions that experience little or no amyloid (e.g., cerebellum, thalamus). If amyloid protein complexes or deposits are toxic to BF cholinergic neurons, this may combine with age-induced oxidative stress to cause their selective vulnerability. In elderly subjects with mild cognitive impairment the Golgi apparatus of BF cholinergic neuron is increased in size, suggesting metabolic activation (Dubelaar et al., 2006). Consistent with this, cortical and hippocampal ChAT activity increases in mild cognitive impairment (DeKosky et al., 2002). It is thought that persons with mild cognitive impairment progress into AD, in which the BF neurons then exhibit a decline in metabolic activity and degenerate (Dubelaar et al., 2004; Salehi et al., 1994). However, excessive amyloid deposition is a feature of only two major brain diseases, AD and Down syndrome. In other diseases in which the BF degenerates one must hypothesize another pathological event or process.

These two major hypotheses of the relevance of BF metabolic activation can be tested in further research. In either case, our study shows that the related projection system in the PPN/LDTN reacts differently to aging. We suggest that further studies contrasting the survival signaling transcriptional systems in these two populations will yield insights into adaptive processes in aging, and how these systems may be compromised in age-related diseases.

## Conflict of interest

There are no actual or potential conflicts of interest for any of the authors.

## Acknowledgements

This work was supported by the Mayo Foundation and NIH grants AG09973 (MM) and GM67825 (PJP). PJP and WRL were also supported by grant U54LM008748, through the NIH Roadmap for Medical Research. PC was supported by an anonomous donor.

## References

Attoor, S., Dougherty, E.R., Chen, Y., Bittner, M., Trent, J.M., 2004. Which is better for cDNA-microarray-based classification: ratios or direct intensities? Bioinformatics 20, 2513–2520.

Baskerville, K.A., Kent, C., Nicolle, M., Gallagher, M., McKinney, M., 2006. Aging causes partial loss of basal forebrain but not brainstem cholinergic neurons. NeuroReport 17, 1819–1823.

Bild, A., Febbo, P.G., 2005. Application of apriori established gene sets to discover biologically important differential expression in microarray data. Proc. Natl. Acad. Sci. USA 102, 15278–15279.

Bonaventure, P., Guo, H., Tian, B., Liu, X., Bittner, A., Roland, B., Salunga, R., Ma, X.-J., Kamme, F., Meurers, B., Bakker, M., Jurzak, M., Leysen, J.E., Erlander, M.G., 2002. Nuclei and subnuclei gene expression profiling in mammalian brain. Brain Res. 943, 38–47.

Cheetham, J.E., Coleman, P.D., Chow, N., 1997. Isolation of single immunohistochemically identified whole neuronal cell bodies from post-mortem human brain for simultaneous analysis of multiple gene expression. J. Neurosci. Methods 77, 43–48.

Chow, N., Cox, C., Callahan, L.M., Weimer, J.M., Guo, L., Coleman, P.D., 1998. Expression profiles of multiple genes in single neurons of Alzheimer's disease. Proc. Natl. Acad. Sci. U.S.A. 95, 9620–9625.

Chung, C.Y., Seo, H., Sonntag, K.C., Brooks, A., Lin, L., Isacson, O., 2005. Cell type-specific gene expression of midbrain dopaminergic neurons reveals molecules involved in their vulnerability and protection. Hum. Mol. Genetics 14, 1709–1725.

Cox, W.G., Beaudet, M.P., Agnew, J.Y., Ruth, J.L., 2004. Possible sources of dye-related signal correlation bias in two-color DNA microarray assays. Anal. Biochem. 331, 243–254.

Curtis, R.K., Oresic, M., Vidal-Puig, A., 2005. Pathways to the analysis of microarray data. Trends Biotechnol. 23, 429–435.

DeKosky, S.T., Ikonomovic, M.D., Styren, S.D., Beckett, L., Wisniewski, S., Bennett, D.A., Cochran, E.J., Kordower, J.H., Mufson, E.J., 2002. Upregulation of choline acetyltransferase activity in hippocampus and frontal cortex of elderly subjects with mild cognitive impairment. Ann. Neurol. 51, 145–155.

Della-Maggiore, V., Sekuler, A.B., Grady, C.L., Bennett, P.J., Sekuler, R., McIntosh, A.R., 2000. Corticolimbic interactions associated with performance on a short-term memory task are modified by age. J. Neurosci. 20, 8410–8416.

Dubelaar, E.G., Mufson, E.J., ter Meulen, W.G., Van Heerikhuize, J.J., Verwer, R.W.H., Swaab, D.F., 2006. Increased metabolic activity in nucleus basalis of Meynert neurons in elderly individuals with mild cognitive impairment as indicated by the size of the Golgi apparatus. J. Neuropathol. Exp. Neurol. 65, 257–266.

Dubelaar, E.J., Verwer, R.W., Hofman, M.A., van Heerikhuize, J.J., Ravid, R., Swaab, D.D., 2004. ApoE epsilon4 genotype is accompainied by lower metabolic activity in nucleus basalis of Meynert neurons in Alzheimer patients and controls as indicated by the size of the Golgi apparatus. J. Neuropathol. Exp. Neurol. 63, 159–169.

Fass, U., Panickar, K., Personett, D., Bryan, D., Williams, K., Gonzales, J., Sugaya, K., McKinney, M., 2000. Differential vulnerability of primary cultured cholinergic neurons to nitric oxide excess. NeuroReport 11, 931–936.

Foster, T.C., 2006. Biological markers of age-related memory deficits. CNS Drug 20, 153–156.

Hernandez, D., McGowan, E., Sugaya, K., Duff, K., McKinney, M., 2001. Survival and plasticity of basal forebrain cholinergic systems in mice transgenic for presenilin-1 and amyloid precursor protein mutant genes. NeuroReport 12, 1377–1384.

Hoekstra, M., Kruijt, J.K., Van Eck, M., Van Berkel, T.J., 2003. Specific gene expression of ATP-binding cassette transporters and nuclear hormone receptors in rat liver parenchymal, endothelial, and Kupffer cells. J. Biol. Chem. 278, 25448–25453.

Livak, K.T., Schmittgen, T.D., 2001. Analysis of relative gene expression data using real-time quantitative PCR and the 2(-Delta Delta C(T)) method. Methods 25, 402–408.

Lo Conte, G., Casamenti, F., Bigl, V., Milaneschi, E., Pepeu, G., 1982. Effect of magnocellular forebrain nuclei lesions on acetylcholine output from the cerebral cortex, electrocorticogram, and behavior. Arch. Ital. Biol. 120, 176–188.

Lottaz, C., Spang, R., 2005. Molecular decomposition of complex clinical phenotypes using biologically structured analysis of microarray data. Bioinformatics 21, 1971–1978.

Lu, T., Pan, Y., Kao, S.-Y., Li, C., Kohane, I., Chan, J., Yanker, B.A., 2004. Gene regulation and DNA damage in the ageing human brain. Nature 429, 883–891.

Luo, L., Salunga, R.C., Guo, H., Bittner, A., Joy, K.C., Galindo, J.E., Xiao, H., Rogers, K.E., Wan, J.S., Jackson, M.R., Erlander, M.G., 1999. Gene expression profiles of laser-captured adjacent neuronal subtypes. Nat. Med. 5, 117–122.

Markham, A., Cameron, I., Franklin, P., Spedding, M., 2004. BDNF increases rat bran mitochondrial respiratory coupling at complex I, but not complex II. Eur. J. Neurosci. 20, 1189–1196.

McKinney, M., 2005. Brain cholinergic vulnerability: relevance to behavior and disease. Biochem. Pharmacol. 70, 1115–1124.

McKinney, M., Baskerville, K., Personett, D., Williams, K., Gonzalez, J., 2003. Cholinergic plasticity and the meaning of death. In: Maiese, K. (Ed.), Neuronal and Vascular Plasticity: Elucidating Basic Cellular Mechanisms for Future Therapeutic Discovery. Kluwer Academic Press, Norwell, MA, pp. 27–74.

McKinney, M., Williams, K., Personett, D., Kent, C., Bryan, D., Gonzalez, J., Baskerville, K., 2004. Pontine cholinergic neurons depend on three neuroprotective systems to resist nitrosative stress. Brain Res. 1002, 100–109.

McKinney, M., Coyle, J.T., 1991. The potential for muscarinic receptor subtype-specific pharmacotherapy for Alzheimer's disease. Mayo Clin. Proc. 66, 1225–1237.

Miasnikov, A.A., Chen, J.C., Weinberger, N.M., 2006. Rapid induction of specific associative behavioral memory by stimulation of the nucleus basalis in the rat. Neurobiol. Learn. Memory 86, 47–65.

Mootha, V.K., Lindgren, C.M., Eriksson, K.F., Subramanian, A., Sihaq, S., Lehar, J., Puiqserver, P., Carlsson, E., Ridderstrale, M., Laurila, E., Houstis, N., Daly, M.J., Patterson, N., Mesirov, J.P., Golub, T.R., Tamayo, P., Spiegelman, B., Lander, E.S., Hirschhorn, J.N., Altshuler, D., Groop, L.C., 2003. PGC-1alpha-responsive genes involved in oxidative phosphorylation are coordinately downregulated in human diabetes. Nat. Genet. 34, 267–273.

Nicolle, M.M., Gonzalez, J., Sugaya, K., Baskerville, K.A., Bryan, D., Lund, K., Gallagher, M., McKinney, M., 2001. Signatures of hippocampal oxidative stress in aged spatial learning-impaired rodents. Neuroscience 107, 415–431.

Ongwijitwat, S., Liang, H.L., Graboyes, E.M., Wong-Riley, M.T.T., 2006. Nuclear respiratory factor 2 senses changing cellular energy demands

and its silencing down-regulates cytochrome oxidase and other target genes. Gene 374, 39–49.

Park, P.J., Cao, Y.A., Lee, S.Y., Kim, J.-W., Chang, M.S., Hart, R., Choi, S., 2004. Current issues for DNA microarrays: platform comparison, double linear amplification, and universal RNA reference. J. Biotechnol. 112, 225–245.

Piantadosi, C.A., Suliman, H.B., 2006. Mitochondrial transcription factor A induction by redox activation of nuclear respiratory factor 1. J. Biol. Chem. 281, 324–333.

Salehi, A., Lucassen, P.J., Pool, C.S., Gonatas, N.K., Ravid, R., Swaab, D.F., 1994. Decreased neurnal activity in the nucleus basalis of Meynert in Alzheimer's disease as suggested by the size of the Golgi apparatus. Neuroscience 59, 871–880.

Scarpulla, R.C., 2006. Nuclear control of respiratory gene expression in mammalian cells. J. Cell. Biochem. 97, 673–683.

Tian, L., Greenberg, S.A., Kong, S.W., Altschuler, J., Kohane, I.S., Park, P.J., 2005. Discovering statistically significant pathways in expression profiling studies. Proc. Natl. Acad. Sci. U.S.A. 102, 13544–13549.

Troyanskaya, O., Cantor, M., Sherlock, G., Brown, P., Hastie, T., Tibshirani, R., Botstein, D., Altman, R.B., 2001. Missing value estimation methods for DNA microarrays. Bioinformatics 17, 520–525.

Van Gelder, R.N., von Zastrow, M.E., Yool, A., Dement, W.C., Barchas, J.D., Eberwine, J.H., 1990. Amplified RNA synthesized from limited quantities of heterogeneous cDNA. Proc. Natl. Acad. Sci. U.S.A. 87, 1663–1667.

Wang, Y., Wang, X., Guo, X.-W., Ghosh, S., 2002. Conditions to ensure competitive hybridization in two-color microarray: a theoretical and experimental analysis. BioTechniques 32, 1342–131346.

Woolf, N.J., Jacobs, R.W., Butcher, L.L., 1989. The pontomesencephalotegmental cholinergic system does not degenerate in Alzheimer's disease. Neurosci. Lett. 96, 277–282.

Yang, S.J., Liang, H.L., Ning, G., Wong-Riley, M.T.T., 2004. Ultrastructural study of depolarization-induced translocation of NRF-2 transcription factor in cultured rat visual cortical neurons. Eur. J. Neurosci. 19, 1153–1162.

Yang, S.J., Liang, H.L., Wong-Riley, M.T.T., 2006. Activity-dependent transcriptional regulation of nuclear respiratory factor-1 in cultured rat visual cortical neurons. Neuroscience 141, 1181–1192.